B. BOZKURT

DYNAMIC ION BEHAVIOR IN PLASMA SOURCE ION IMPLANTATION

BİLGE BOZKURT

JANUARY 2006

METU 2006

DYNAMIC ION BEHAVIOR IN PLASMA SOURCE ION IMPLANTATION

A THESIS SUBMITTED TO
THE GRADUATE SCHOOL OF NATURAL AND APPLIED SCIENCES
OF
MIDDLE EAST TECHNICAL UNIVERSITY

BY

BİLGE BOZKURT

IN PARTIAL FULFILLMENT OF THE REQUIREMENTS
FOR
THE DEGREE OF MASTER OF SCIENCE
IN
PHYSICS

JANUARY 2006

Approval of the Graduate School of Natural and Applied Sciences

Prof. Dr. Canan Özgen
Director

I certify that this thesis satisfies all the requirements as a thesis for the degree of Master of Science.

Prof. Dr. Sinan Bilikmen
Head of Department

This is to certify that we have read this thesis and that in our opinion it is fully adequate, in scope and quality, as a thesis for the degree of Master of Science.

Prof. Dr. Sinan Bilikmen
Supervisor

Examining Committee Members

Prof. Dr. Arif Demir	(Kocaeli Unv, PHYS)	———
Prof. Dr. Sinan Bilikmen	(METU, PHYS)	———
Assist. Prof. Dr. İsmail Rafatov	(METU, PHYS)	———
Assoc. Prof. Dr. Akif Esendemir	(METU, PHYS)	———
Assoc. Prof. Dr. Serhat Çakır	(METU, PHYS)	———

I hereby declare that all information in this document has been obtained and presented in accordance with academic rules and ethical conduct. I also declare that, as required by these rules and conduct, I have fully cited and referenced all material and results that are not original to this work.

Name, Last name: Bilge Bozkurt

Signature :

ABSTRACT

DYNAMIC ION BEHAVIOR IN PLASMA SOURCE ION IMPLANTATION

Bozkurt, Bilge
M. S., Department of Physics
Supervisor: Prof. Dr. Sinan Bilikmen

January 2006, 74 pages

The aim of this work is to analytically treat the dynamic ion behavior during the evolution of the ion matrix sheath, considering the industrial application plasma source ion implantation for both planar and cylindrical targets, and then to develop a code that simulates this dynamic ion behavior numerically. If the separation between the electrodes in a discharge tube is small, upon the application of a large potential between the electrodes, an ion matrix sheath is formed, which fills the whole inter-electrode space. After a short time, the ion matrix sheath starts moving towards the cathode and disappears there. Two regions are formed as the matrix sheath evolves. The potential profiles of these two regions are derived and the ion flux on the cathode is estimated. Then, by using the finite-differences method, the problem is simulated numerically. It has been seen that the results of both analytical calculations and numerical simulations are in a good agreement.

Keywords: Ion implantation, Plasma Source Ion Implantation, Plasma Immersion Ion Implantation, Dynamic Ion Behavior, Modeling

ÖZ

PLAZMA KAYNAKLI İYON EKİMİNDE DİNAMİK İYON HAREKETİ

Bozkurt, Bilge
Yüksek Lisans, Fizik Bölümü
Tez Yöneticisi: Prof. Dr. Sinan Bilikmen

Ocak 2006, 74 sayfa

Bu çalışmanın amacı, plazma kaynaklı iyon ekimi ile düzlemsel ve silindirik hedefler için endüstriyel uygulama düşünülerek iyon-matris plakalarının evrimi esnasındaki dinamik iyon hareketini analitik olarak çalışmak ve sonra bu dinamik iyon hareketini sayısal olarak simüle eden bir kod geliştirmektir. Eğer bir deşarj tüpünde elektrotlar arası mesafe az ise, elektrotlar arasına yüksek bir potansiyel uygulandığında, tüm elektrotlar arası mesafeyi dolduran bir iyon-matris plakası oluşur. Kısa bir süre sonra iyon-matris plakası katoda doğru hareket etmeye başlar ve orada kaybolur. Matris plakasının evrimi esnasında iki bölge oluşur. Bu iki bölgenin potansiyel profili türetilmiş ve katottaki iyon akısı hesap edilmiştir. Sonra, sonlu farklar metodu kullanılarak problem sayısal olarak simüle edilmiştir. Analitik hesaplamaların sonuçları ile sayısal simülasyonların uyumlu olduğu gözlemlenmiştir.

Anahtar Kelimeler: İyon Ekimi, Plazma Kaynaklı İyon Ekimi, Dinamik İyon Hareketi, Sayısal Çözümleme, Modelleme

FOR PROF. DR. ORDAL DEMOKAN

ACKNOWLEDGEMENTS

I would like to express my deepest gratitude to dear Prof. Dr. Ordal Demokan for suggesting this research and his guidance, advice, support and insight in this study until his sorrowful demise.

I would like to express my gratitude to my supervisor Prof. Dr. Sinan Bilikmen for his guidance, suggestions, comments, contribution and support.

I would also like to express my grateful thanks to Assist. Prof. Dr. İsmail Rafatov and Prof. Dr. Ayşe Karasu for their guidance, contributions and suggestions.

I would like to thank my family and my fiancé for their moral support and encouragement.

I would also like to thank İnanç Kanık and Yasemin Filiz for their invaluable discussions, suggestions, comments and support.

TABLE OF CONTENTS

LIST OF FIGURES

FIGURES

CHAPTER 1

INTRODUCTION

1.1. Plasma Processing

Plasma processing is a plasma-based material processing technology, the aim of which is to modify the properties of the surfaces of materials such as metals, plastics and ceramics by various processes like deposition, implantation, and etching etc [1] – [3].

The principal component of plasma processing is the plasma medium, in which the material to be processed is immersed. To maintain the desired plasma medium, generally DC and radio frequency (RF) discharges are used. RF discharges are used for a broad range of processes such as deposition, etching and treatment while DC discharges are preferred in ion implantation processes as DC discharges involve large potentials [1].

The applications of plasma processing include: the manufacturing of integrated circuits; the decontamination of waste materials and surfaces; plasma source ion implantation and the etching of silicon wafers for semiconductor fabrication [2, 4].

1.2. Plasma Source Ion Implantation

Plasma source ion implantation (PSII), which was invented by Conrad in 1987 [3], has become well-known as one of the well-established plasma-based manufacturing technique, frequently used in the surface modification of materials for industrial applications [5] – [8].

PSII is a room temperature surface enhancement technique that uses a plasma medium surrounding a target and high-negative-voltage, high-current pulses to accelerate ions into a target surface from all directions. PSII modifies the target surface in beneficial ways, making it harder, improving wear properties, reducing the coefficient of friction, enhancing its resistance to corrosion and dramatically improving the wear-life of manufacturing tools in actual industrial applications. The block diagram of a typical PSII system is given in figure 1.1 [9] – [11].

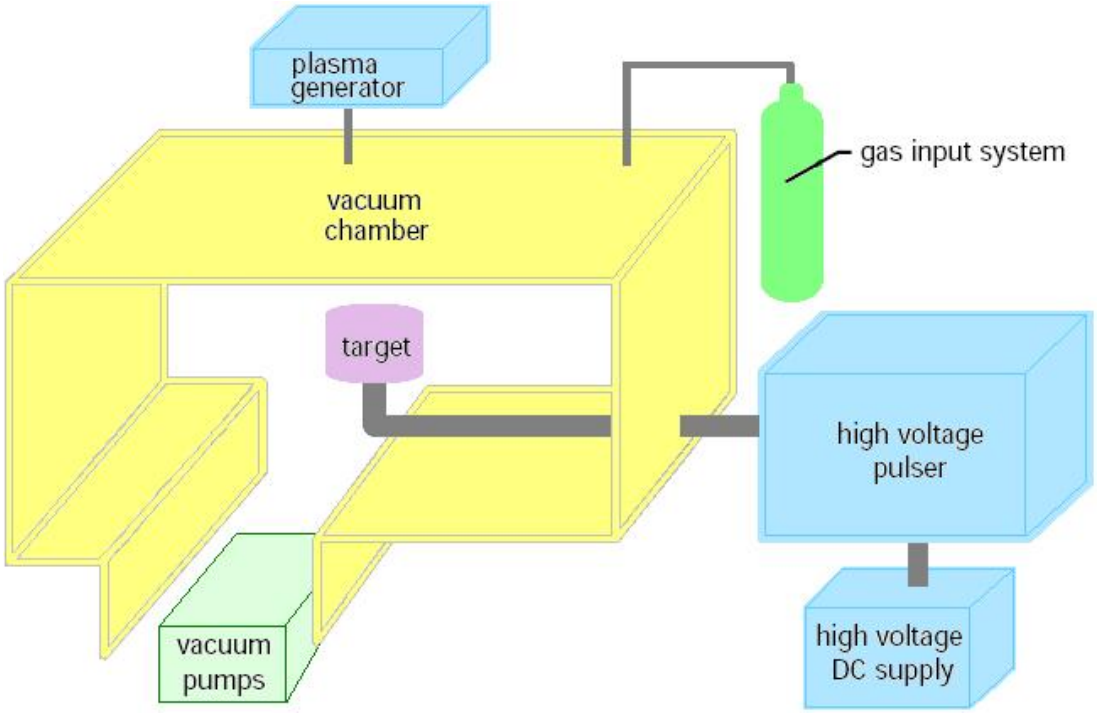

Figure 1.1: Block diagram of a typical PSII system.

PSII departs radically from conventional ion implantation technology in the following aspects [7, 10, 11]:

1. In PSII, targets are placed directly into a plasma medium and ions are accelerated onto the target through a plasma sheath that surrounds the target. Hence, PSII is a non-line-of-sight technique which means a path from a single ion source to the surface of the target is not required. This enables PSII to treat the entire target surface simultaneously without the need of the time-consuming rotation of the target and to treat multiple target surfaces simultaneously without the need for in-vacuum manipulation of the target assembly.
2. In PSII, the ions are accelerated normal to the surface of the target so there is no retained dose problem. Even with target rotation, the conventional ion implantation technique requires target masking in order to minimize the grazing incidence, which produces excessive sputtering, and therefore limits the retained dose.
3. PSII is not limited by ion optics characteristics or by the Child-Langmuir space charge limited flow properties of conventional ion implantation techniques. Due to this fact, the average ion flux to the target surface can be more than an order of magnitude larger than using conventional techniques at low energies, which significantly reduces the required treatment time for large, complex target assemblies and enables PSII to implant ions efficiently to concentrations and depths required for surface modification.
4. PSII is a simple and low-cost technique because at the ion accelerator stage, the target rotation apparatus is eliminated in PSII.
5. Since the target rotation stage does not exist in PSII, large and heavy targets can also be treated by PSII. The target rotation in conventional ion implantation technique adds complexity to the process and reduces the size of the target.
6. PSII is a room temperature process. The rotation problem in the conventional ion implantation technique is aggravated by the need for adequate heat sinks at the targets to limit the temperature rise during implantation.
7. It has high dose rates, intrinsic charge neutralization capability, and adaptability to other surface modification processes.

1.3. Basic Plasma Sheath Physics

In the PSII technique, the material, whose surface is to be modified, acts as the cathode in a grounded vacuum chamber, in which a flow of the gas required for implantation is maintained. The gas inside the vacuum chamber is ionized by one of the various discharge methods [5, 6, 7, 11].

1.3.1. Phase 1

When a large negative step potential or a train of high voltage negative pulses, $-\Phi$, that has a magnitude between 10 kV and 100 kV is applied to the cathode at time $t = 0$, the electrons are quickly repelled from the cathode on the time scale of electron plasma frequency ($1/\omega_{pe}$) as shown in figure 1.2 [5] – [7]. On this time scale, as electrons recede, the ions' motion is negligible so that the repelled electrons leave behind an electron-free region, namely the ion matrix sheath [11]. The ion matrix sheath consists of uniformly distributed, stationary ions, conformally mapping the cathode surface, which is shown in figure 1.3 [5] – [7]. An ion matrix sheath is a region between a quasi-neutral plasma and a negative electrode to which a large negative step potential, $-\Phi$, is applied [11].

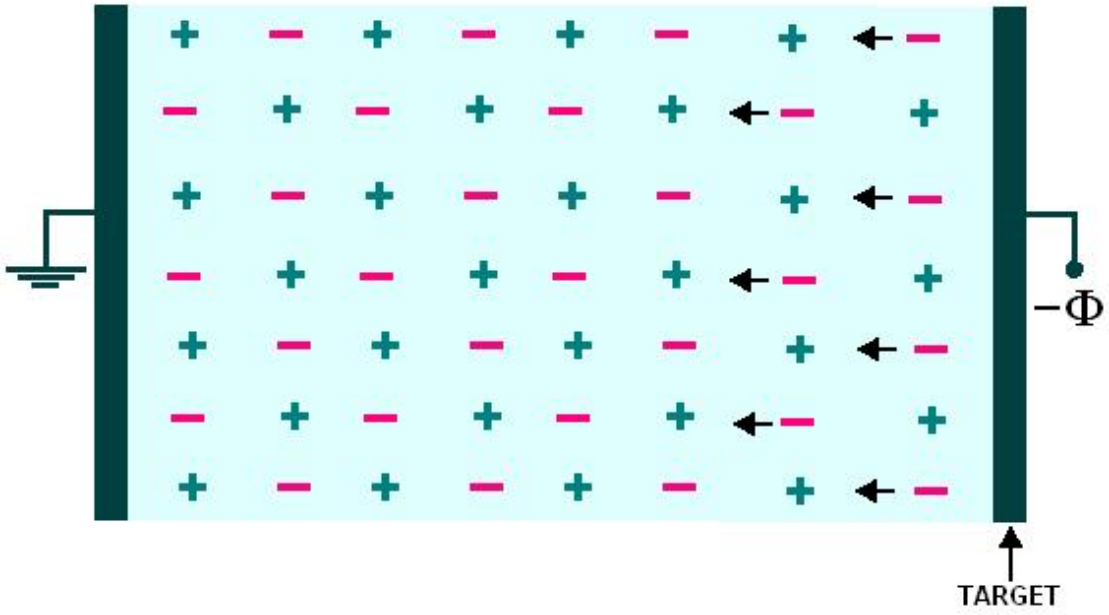

Figure 1.2: When a large negative step potential or a train of high voltage negative pulses, $-\Phi$, is applied to the cathode, electrons are quickly repelled from the cathode on the time scale of electron plasma frequency.

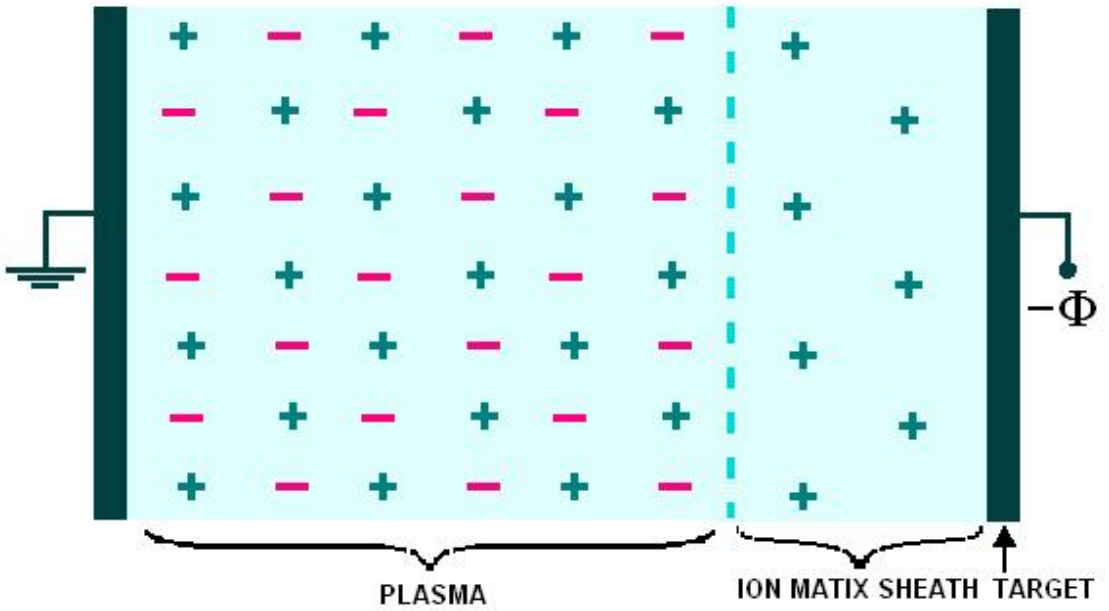

Figure 1.3: An ion-matrix sheath is left behind.

1.3.2. Phase 2

After a time scale of the ion plasma frequency ($1/\omega_{pi}$), the ions start responding to the sheath electric field and start to accelerate towards the cathode [5] – [7], which is usually the target in PSII. The decreasing ion density in the sheath region causes a decrease in the electron density [11] and consequently the sheath starts expanding at approximately the ion acoustic velocity towards the Child– Langmuir limit, uncovering ions which are then accelerated towards the cathode by the field in the sheath [5] – [7], which is shown in figure 1.4.

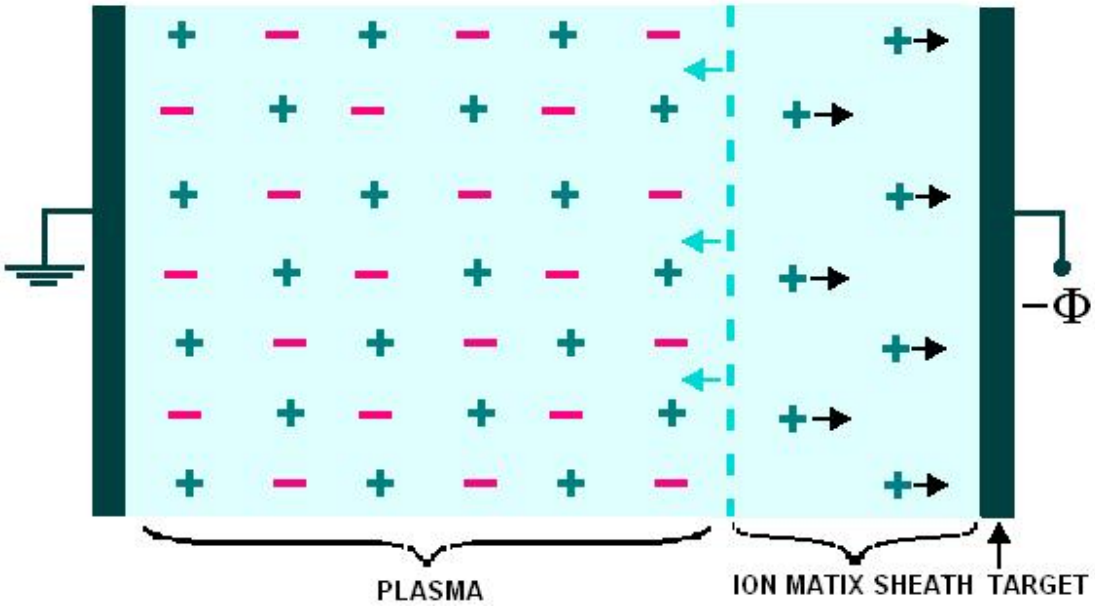

Figure 1.4: After a time scale of the ion plasma frequency, ions start responding and the ion matrix sheath starts to expand.

These ions eventually bombard the target cathode perpendicularly and uniformly, with sufficient energies to produce implantation. The experimental and numerical

[12] – [15] investigations show that the ion-matrix phase plays a vital role in determining the consequent ion flux to the target surface [5, 6, 11].

1.3.3. Phase 3

After the sheath edge reaches the Child-Langmuir limit, it stops expanding and launches an ion-acoustic wave into the plasma, which produces ion rarefication as it propagates. This rarefication creates a quasi-neutral presheath region between the plasma and the sheath, which accelerates ions up to Bohm's speed before entering the sheath. The potential profile in this state is given in figure 1.5.

Figure 1.5: The steady state potential profile.

Sheath voltages are often very large compared to the electron temperature, T_e. The potential Φ in ion matrix sheaths is highly negative with respect to the plasma-sheath edge; hence $n_e \sim n_s e^{\Phi/T_e} \to 0$ where n_e is the electron density and n_s is the density of electrons at the sheath edge, which means that there are only ions in the matrix sheath. Therefore, for a high-voltage sheath, the current at the cathode is almost all ion current [16].

1.4. The Objectives and Content of the Thesis

Theoretical investigations of ion-matrix sheaths for planar, cylindrical, and spherical targets have been successfully carried out by Conrad [11], where the planar and cylindrical targets were assumed to have infinite areas and lengths, respectively, reducing the analysis to one-dimensional cases [5]. Sheridan [17] and Zeng [18] have applied the same formulation to study the ion-matrix sheaths in cylindrical bores, with and without axial electrodes, respectively. Demokan [7] and Filiz [4] presented the first analytic treatments of ion-matrix sheaths in two dimensions, by considering first a rectangular and then a semi-cylindrical groove of infinite lengths in an infinite, planar target. Finally, Demokan [5] represented the problem of ion matrix sheaths inside cylindrical bores with small radii and longitudinal grooves analytically, which treated the problem more realistically to promote the application of plasma source ion implantation techniques to a broad range of products, especially those concerning defense industries. However, for the targets considered in his work, implantation on the side walls of the grooves is relatively poor, since the ions are accelerated predominantly in the radial direction before entering the grooves [5]. In his paper Demokan suggested maximizing the ratio of the ion velocity components inside the grooves by using a new technique, increasing the ratio $\frac{n_0}{\Phi_0}$ (where n_0 is initial ion density and Φ_0 is the target potential) and letting the inter-electrode space approximately equal the target radius times the target potential.

In this thesis, a new analytical technique to study the evolution of ion matrix sheaths will be examined for planar and cylindrical configurations, a computer program will be developed to simulate the sheath evolution numerically and a basis for future studies on the problem of cylindrical bores with small radii and grooves will be established.

CHAPTER 2

THEORY AND CALCULATIONS

2.1. PLANAR CONFIGURATION

2.1.1. The Model

The problem, subject to our work is illustrated in figures 2.1, 2.2 and 2.3, considering the initial phase and the proceeding evolution.

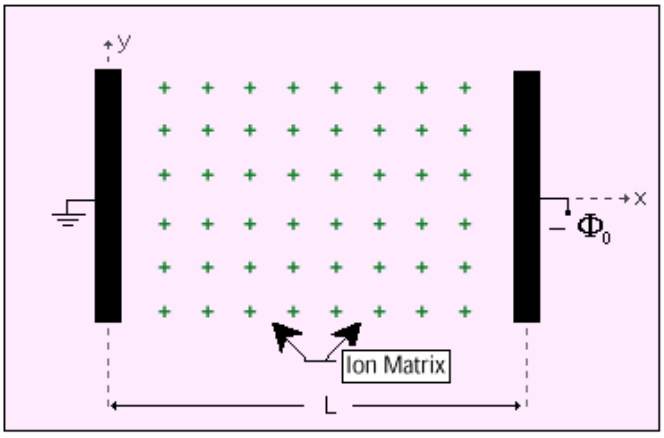

Figure 2.1: When the applied potential, $-\Phi_0$, is large (~ 20 kV) and the electrode separation is small (~ 10^{-2} m), the matrix can fill the entire inter-electrode space ($1/\omega_{pe} < t < 1/\omega_{pi}$), where ω_{pe} and ω_{pi} are electron and ion plasma frequencies, respectively.

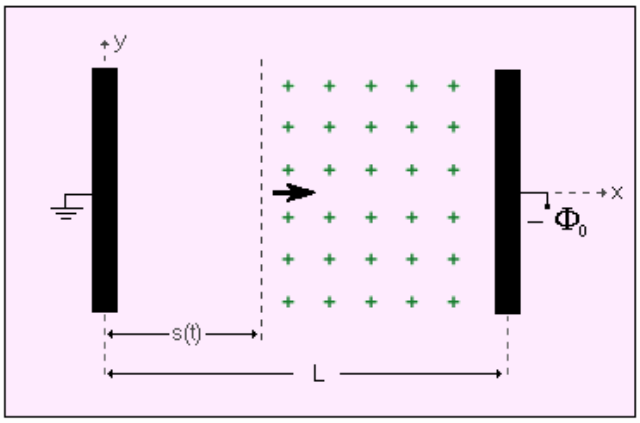

Figure 2.2: After a short time, the matrix starts moving towards the cathode. The notation $s(t)$ represents the time-dependent location of the sheath edge.

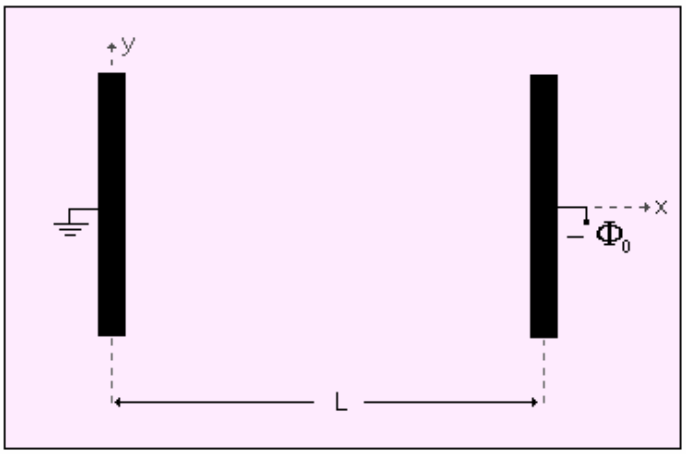

Figure 2.3: The matrix disappears as all ions are implanted.

The model presented here is a one-dimensional model, with a planar anode of infinite area placed at $x = 0$ and a planar cathode where the target to be implanted is placed at $x = L$. The target considered is also a planar plate that has an infinite

area. The magnitude of L is ~ 10^{-2} m. The negative potential applied to the cathode is ~ 20 kV, whereas the anode is kept at zero potential. Potential for $0 < x < s(t)$ is labeled as $\Phi_>$ and the potential for $s(t) < x < L$ is labeled as $\Phi_<$.

The following assumptions have been made:

1) The ion density n, the potentials $\Phi_<$ and $\Phi_>$, and the ion velocity u_i have a form, which is a zeroth order term that does not take into account the contributions from the ion density plus a first order term due to the contributions from the ion density;

2) Since the contribution of n is already a first order term, any fluctuation in this term is a second order term, and can be neglected in Poisson's Equation;

3) However, both $\Phi_<$ and $\Phi_>$ will be time dependent due to $s(t)$.

Therefore,

$$\Phi_< = \Phi_<^{(0)} + \Phi_<^{(1)}, \tag{2.1.1}$$

$$\Phi_> = \Phi_>^{(0)} + \Phi_>^{(1)}, \tag{2.1.2}$$

$$n = n^{(1)} = n_0, \tag{2.1.3}$$

$$u_i = u_i^{(0)} + u_i^{(1)}. \tag{2.1.4}$$

2.1.2. The Determination of Potentials

To determine the potentials in both regions $0 < x < s(t)$ and $s(t) < x < L$, the Poisson's equations in these regions have to be solved and the boundary conditions have to be imposed.

Since the zeroth order potentials, $\Phi_{>}^{(0)}$ and $\Phi_{<}^{(0)}$, neglect the effect of n, which is a first order term, they are equal, $\Phi_{>}^{(0)}(x) = \Phi_{<}^{(0)}(x)$, and the first order potentials $\Phi_{>}^{(1)}$ and $\Phi_{<}^{(1)}$ will depend on time.

The Poisson's Equations for $\Phi_{>}^{(0)}$ and $\Phi_{<}^{(0)}$ are

$$\frac{\partial^2 \Phi_{>}^{(0)}}{\partial x^2} = 0\,, \tag{2.1.5}$$

$$\frac{\partial^2 \Phi_{<}^{(0)}}{\partial x^2} = 0\,. \tag{2.1.6}$$

The boundary conditions to be imposed for $\Phi_{>}^{(0)}$ and $\Phi_{<}^{(0)}$ are

$$x = 0\,, \qquad \Phi_{>}^{(0)}(0) = 0\,, \tag{2.1.7}$$

$$x = L\,, \qquad \Phi_{>}^{(0)}(L) = \Phi_{<}^{(0)}(L) = -\Phi_0\,. \tag{2.1.8}$$

Then, the solutions for $\Phi_{>}^{(0)}$ and $\Phi_{<}^{(0)}$ are found as

$$\Phi_{>}^{(0)}(x) = \Phi_{<}^{(0)}(x) = -\frac{\Phi_0}{L}x\,. \tag{2.1.9}$$

The Poisson's equations for $\Phi_{>}^{(1)}$ and $\Phi_{<}^{(1)}$ are

$$\frac{\partial^2 \Phi_{>}^{(1)}}{\partial x^2} = 0\,, \tag{2.1.10}$$

$$\frac{\partial^2 \Phi_{<}^{(1)}}{\partial x^2} = -\frac{en^{(1)}}{\varepsilon_0} = -\frac{en_0}{\varepsilon_0}\,. \tag{2.1.11}$$

The boundary conditions to be imposed for $\Phi_{>}^{(1)}$ and $\Phi_{<}^{(1)}$ are

$$x = 0\,, \qquad \Phi_{>}^{(1)}(0,t) = 0\,, \tag{2.1.12}$$

$$x = s(t)\,, \qquad \Phi_{>}^{(1)}(x,t)\Big|_{s(t)} = \Phi_{<}^{(1)}(x,t)\Big|_{s(t)}\,, \tag{2.1.13}$$

$$x = s(t)\,, \qquad \left.\frac{\partial \Phi_{>}^{(1)}}{\partial x}\right|_{s(t)} = \left.\frac{\partial \Phi_{<}^{(1)}}{\partial x}\right|_{s(t)}\,, \tag{2.1.14}$$

$$x = L\,, \qquad \Phi_{<}^{(1)}(L,t) = 0 \tag{2.1.15}$$

Then, the solutions for $\Phi_{>}^{(1)}$ and $\Phi_{<}^{(1)}$ are found as

$$\Phi_{>}^{(1)}(x,t) = \frac{en_0}{2\varepsilon_0 L}\big(L - s(t)\big)^2 x\,, \tag{2.1.16}$$

$$\Phi_{<}^{(1)}(x,t) = -\frac{en_0}{2\varepsilon_0}x^2 + \frac{en_0}{2\varepsilon_0 L}\Big[\big(s(t)\big)^2 + L^2\Big]x - \frac{en_0}{2\varepsilon_0}\big(s(t)\big)^2\,. \tag{2.1.17}$$

Therefore, the potentials in the regions $0 < x < s(t)$ and $s(t) < x < L$, i.e. $\Phi_{>}$ and $\Phi_{<}$, are found as

$$\Phi_{>}(x,t) = -\frac{\Phi_0}{L}x + \frac{en_0}{2\varepsilon_0 L}\big(L - s(t)\big)^2 x\,, \tag{2.1.18}$$

$$\Phi_{<}(x,t) = -\frac{\Phi_0}{L}x - \frac{en_0}{2\varepsilon_0}x^2 + \frac{en_0}{2\varepsilon_0 L}\Big[\big(s(t)\big)^2 + L^2\Big]x - \frac{en_0}{2\varepsilon_0}\big(s(t)\big)^2\,. \tag{2.1.19}$$

These potentials do not depend on time explicitly. To find the explicit time dependence of the potentials, the explicit form of $s(t)$ must be determined.

To do this, the equation of motion at $x = s(t)$ is used, which is

$$m\frac{d^2 s}{dt^2} = -e\frac{\partial \Phi_>}{\partial x}\bigg|_{x=s(t)} . \tag{2.1.20}$$

Substituting $\Phi_>$ gives

$$\frac{d^2 s}{dt^2} = \frac{e\Phi_0}{mL}\left[1 - \frac{en_0 L^2}{2\Phi_0 \varepsilon_0}\left(\frac{s(t)}{L} - 1\right)^2\right]. \tag{2.1.21}$$

To be consistent, $s(t)$ is also assumed to have a form $s(t) = s^{(0)}(t) + s^{(1)}(t)$.

$$\frac{d^2 s}{dt^2} = \frac{d^2 s^{(0)}}{dt^2} + \frac{d^2 s^{(1)}}{dt^2} = \frac{e\Phi_0}{mL}\left[1 - \frac{en_0 L^2}{2\Phi_0 \varepsilon_0}\left(\frac{s^{(0)}(t)}{L} + \frac{s^{(1)}(t)}{L} - 1\right)^2\right] \tag{2.1.22}$$

To find the zeroth and first order terms in this differential equation, let us examine the potential $\Phi_<$. Since $\Phi_<^{(0)}(x) = \Phi_>^{(0)}(x) = -\frac{\Phi_0}{L}x$, the zeroth order equation of motion is

$$\frac{d^2 s^{(0)}}{dt^2} = \frac{e\Phi_0}{mL} \tag{2.1.23}$$

which gives

$$\frac{ds^{(0)}}{dt} = u_i^{(0)} = \frac{e\Phi_0}{mL}t . \tag{2.1.24}$$

Rearranging its terms, equation (2.1.17) becomes

$$\Phi_{<}^{(1)}(x,t) = -\frac{en_0 x}{2\varepsilon_0}\left[L + \frac{(s(t))^2}{L} - x - \frac{(s(t))^2}{x}\right]. \qquad (2.1.26)$$

The terms in brackets have a maximum value of $\left[L + \frac{(s(t))^2}{L} - x - \frac{(s(t))^2}{x}\right]_{\max} = L$.

Then, $\Phi_{<}^{(1)}$ is on the order of $\frac{en_0 xL}{2\varepsilon_0}$, which gives $\left|\frac{\Phi_{<}^{(1)}}{\Phi_{<}^{(0)}}\right| \le \frac{en_0 L^2}{2\Phi_0\varepsilon_0}$. So, $\frac{en_0 L^2}{2\Phi_0\varepsilon_0} \langle\langle 1$ is a first order term.

Then, the zeroth order equation of motion is given by equation (2.1.23) and the first order equation of motion is given by

$$\frac{d^2 s^{(1)}}{dt^2} = -\frac{e\Phi_0}{mL}\frac{en_0 L^2}{2\Phi_0\varepsilon_0}\left(\frac{s^{(0)}(t)}{L} - 1\right)^2 \qquad (2.1.26)$$

Therefore, from the differential equations (2.1.23) and (2.1.26), $s^{(0)}(t)$ and $s^{(1)}(t)$ are found as given in equations (2.1.27) and (2.1.28).

$$s^{(0)}(t) = \frac{e\Phi_0}{2mL}t^2 \qquad (2.1.27)$$

$$s^{(1)}(t) = -\frac{e\Phi_0 A^2}{2mL}t^2 + \frac{e^2(\Phi_0)^2 A^2}{12m^2L^3}t^4 - \frac{e^3(\Phi_0)^3 A^2}{120m^3L^5}t^6 \qquad (2.1.28)$$

where $A^2 = \frac{en_0 L^2}{2\Phi_0\varepsilon_0}$, which is a first order term.

To compare these terms, maximum time, $t_{\max}$, involved in this process must be estimated. Then, $s^{(0)}(t_{\max}) \approx L \approx \frac{e\Phi_0}{2mL}(t_{\max})^2$ gives

$$t_{\max} \cong \left[\frac{2mL^2}{e\Phi_0}\right]^{1/2} . \tag{2.1.29}$$

So, the terms in $s^{(1)}(t)$, in equation (2.1.28), correspond to 1, 1/3, 1/15, respectively. Then, the first two terms can be considered of equal order and $s(t)$ is found as given

$$s(t) = \frac{e\Phi_0}{2mL}\left[1 - A^2 + \frac{e\Phi_0 A^2}{6mL^2}t^2\right] t^2 . \tag{2.1.30}$$

Neglecting the second order terms, which come from the square of A^2, the explicit forms of the potentials $\Phi_>$ and $\Phi_<$ are given by

$$\begin{aligned}\Phi_>(x,t) = &-\frac{\Phi_0}{L}x + \frac{en_0L}{2\varepsilon_0}x - \frac{e^2n_0\Phi_0}{2\varepsilon_0 mL}\left(1-A^2\right)xt^2 \\ &+ \frac{e^3n_0(\Phi_0)^2}{\varepsilon_0 m^2L^3}\left(\frac{1}{8}-\frac{A^2}{3}\right)xt^4 + \frac{e^4n_0(\Phi_0)^3}{24\varepsilon_0 m^3L^4}A^2xt^6\end{aligned} , \tag{2.1.31}$$

$$\begin{aligned}\Phi_<(x,t) = &-\frac{\Phi_0}{L}x - \frac{en_0}{2\varepsilon_0}x^2 + \frac{en_0L}{2\varepsilon_0}x \\ &+ \frac{e^3n_0(\Phi_0)^2}{8\varepsilon_0 m^2L^3}\left(1-2A^2\right)xt^4 - \frac{e^3n_0(\Phi_0)^2}{8\varepsilon_0 m^2L^2}\left(1-2A^2\right)t^4 . \\ &+ \frac{e^4n_0(\Phi_0)^3}{24\varepsilon_0 m^3L^5}A^2xt^6 - \frac{e^4n_0(\Phi_0)^3}{24\varepsilon_0 m^3L^4}A^2t^6\end{aligned} \tag{2.1.32}$$

2.1.3. The Determination of Ion Velocity and Flux

To examine the ion behavior, the ion velocity and the flux must be determined. To do this, the equation of motion is considered.

$$\frac{du_i}{dt} = \frac{\partial u_i}{\partial t} + u_i \frac{\partial u_i}{\partial x} = -\frac{e}{m}\frac{\partial \Phi_<}{\partial x}. \tag{2.1.33}$$

Substituting equations (2.1.4) and (2.1.32), i.e. $u_i(x,t)$ and $\Phi_<(x,t)$, the zeroth and first order equations of the ion velocity can be found as given by equations (2.1.34) and (2.1.35).

$$\frac{\partial u_i^{(0)}}{\partial t} + u_i^{(0)} \frac{\partial u_i^{(0)}}{\partial x} = \frac{e\Phi_0}{mL} \tag{2.1.34}$$

$$\frac{\partial u_i^{(1)}}{\partial t} + u_i^{(1)} \frac{\partial u_i^{(0)}}{\partial x} + u_i^{(0)} \frac{\partial u_i^{(1)}}{\partial x} = \frac{e^2 n_o}{\varepsilon_0 m} x - \frac{e^5 (\Phi_0)^3 n_0 A^2}{24\varepsilon_0 m^4 L^5} t^6 - \frac{e^4 (\Phi_0)^2 n_0 (1-2A^2)}{8\varepsilon_0 m^3 L^3} t^4 - \frac{e^2 n_o L}{2\varepsilon_0 m} \tag{2.1.35}$$

Since the right hand side of equation (2.1.34) is a constant, this differential equation can be written as $\frac{du_i^{(0)}}{dt} = \frac{e\Phi_0}{mL}$, and imposing the initial condition $u_i^{(0)}(x,0) = 0$, it has a solution in the form

$$u_i^{(0)}(t) = \frac{e\Phi_0}{mL} t. \tag{2.1.36}$$

Substituting this solution, equation (2.1.36), into equation (2.1.35), the differential equation becomes

$$\frac{\partial u_i^{(1)}}{\partial t}+\frac{e\Phi_0}{mL}t\frac{\partial u_i^{(1)}}{\partial x}=\frac{e^2 n_o}{\varepsilon_0 m}x-\frac{e^5(\Phi_0)^3 n_0 A^2}{24\varepsilon_0 m^4 L^5}t^6 - \frac{e^4(\Phi_0)^2 n_0(1-2A^2)}{8\varepsilon_0 m^3 L^3}t^4-\frac{e^2 n_o L}{2\varepsilon_0 m} \quad . \tag{2.1.37}$$

The solution of a quasi-linear equation of first order that has a general form of $P(x,t)\frac{\partial u(x,t)}{\partial x}+Q(x,t)\frac{\partial u(x,t)}{\partial t}=R(u,x,t)$ is found by the method of characteristics, that is by simultaneously solving the equations $\frac{dx}{P}=\frac{dt}{Q}=\frac{du}{R}$.

Applying this method to our differential equation, equation (2.1.37), and imposing the initial condition, $u_i^{(1)}(x,0)=0$, the solution is found to be

$$u_i^{(1)}(x,t)=\frac{e^2 n_o}{\varepsilon_0 m}xt-\frac{e^2 n_o}{\varepsilon_0 m}\frac{e\Phi_0}{mL}\frac{t^3}{3}-\frac{e^5(\Phi_0)^3 n_0 A^2}{24\varepsilon_0 m^4 L^5}\frac{t^7}{7} - \frac{e^4(\Phi_0)^2 n_0(1-2A^2)}{8\varepsilon_0 m^3 L^3}\frac{t^5}{5}-\frac{e^2 n_o L}{2\varepsilon_0 m}t \quad . \tag{2.1.38}$$

Using the estimated value of maximum time, $t_{\max}$, involved in this process, which is given by equation (2.1.29), the terms of $u_i^{(1)}(x,t_{\max})$ are compared with the term of $u_i^{(0)}(t_{\max})$ and the coefficients of t^5 and t^7 are found to be negligible. Then, the first order ion velocity becomes

$$u_i^{(1)}(x,t)=\frac{e^2 n_o}{\varepsilon_0 m}xt-\frac{e^2 n_o}{\varepsilon_0 m}\frac{e\Phi_0}{mL}\frac{t^3}{3}-\frac{e^2 n_o L}{2\varepsilon_0 m}t \quad . \tag{2.1.39}$$

Combining equations (2.1.36) and (2.1.39), the ion velocity has the form

$$u_i(x,t) = \left(\frac{e\Phi_0}{mL} - \frac{e^2 n_o L}{2\varepsilon_0 m} \right) t + \frac{e^2 n_o}{\varepsilon_0 m} xt - \frac{e^2 n_o}{\varepsilon_0 m} \frac{e\Phi_0}{mL} \frac{t^3}{3}. \qquad (2.1.40)$$

Therefore, the ion flux has the form

$$\begin{aligned} \Gamma(x,t) &= n_0 u_i(x,t) \\ &= \left(\frac{e n_0 \Phi_0}{mL} - \frac{e^2 (n_0)^2 L}{2\varepsilon_0 m} \right) t + \frac{e^2 (n_o)^2}{\varepsilon_0 m} xt - \frac{e^2 (n_o)^2}{\varepsilon_0 m} \frac{e\Phi_0}{mL} \frac{t^3}{3}. \end{aligned} \qquad (2.1.41)$$

2.1.4. Graphical Representation

The ion velocity is given by equation (2.1.40). At a particular time t, this ion velocity has a form $u_i(x)\big|_t = Cx + D$ where C and D are constants. In figures 2.4, 2.5, 2.6, and 2.7, this almost linear dependence is shown graphically at $t = \frac{t_{\max}}{4}$, $t = \frac{t_{\max}}{2}$, $t = \frac{3t_{\max}}{4}$, and $t = t_{\max}$, respectively.

In the calculations, the ions are assumed to be titanium ions and the ion mass is taken to be $48 \times 1.67 \times 10^{-27}$ kg. Also in the calculations, the magnitude of the distance between the electrodes, L, is taken to be ~ 10^{-2} m, the negative potential applied to the cathode, Φ_0, is taken to be ~ 20 kV, potential applied to the anode is taken to be 0.0 kV, the initial ion velocity is taken to be 0.0 m/s and the initial ion density, n_0, is taken to be ~ 10^{15} /m^3.

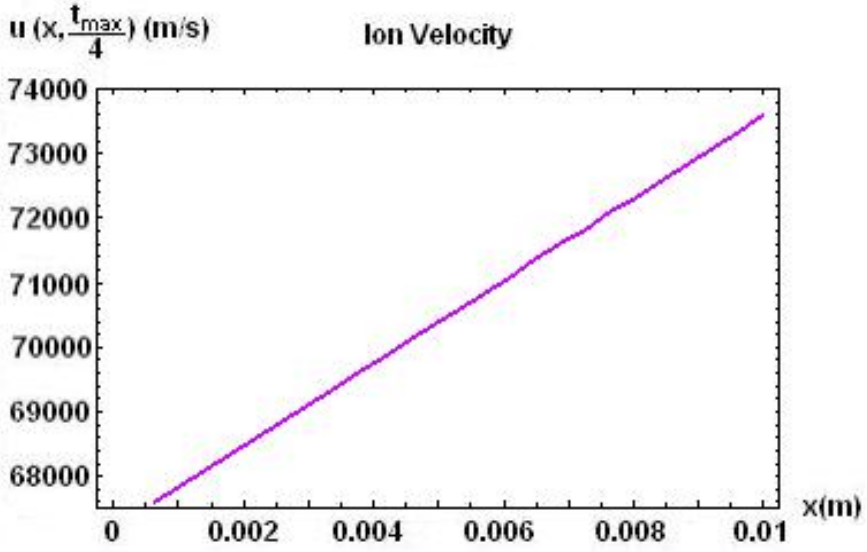

Figure 2.4: Ion velocity as a function of x at time $t = t_{\max}/4$.

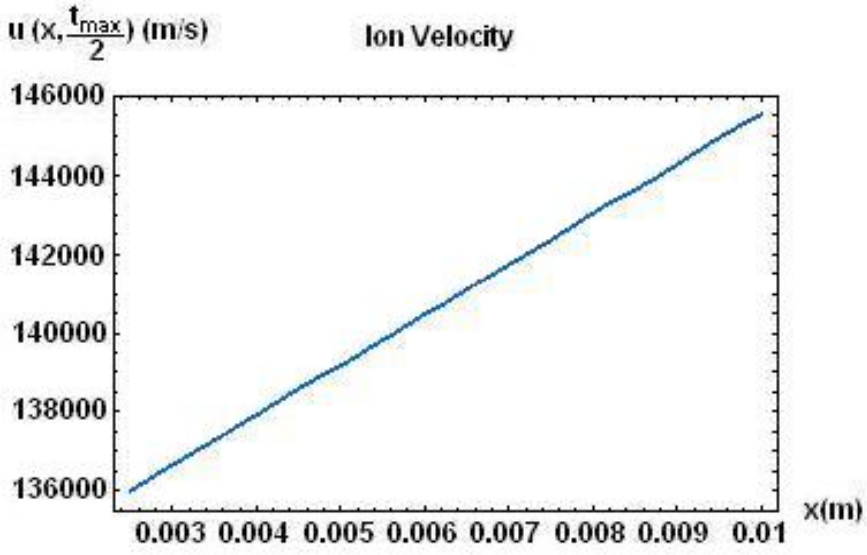

Figure 2.5: Ion velocity as a function of x at time $t = t_{\max}/2$.

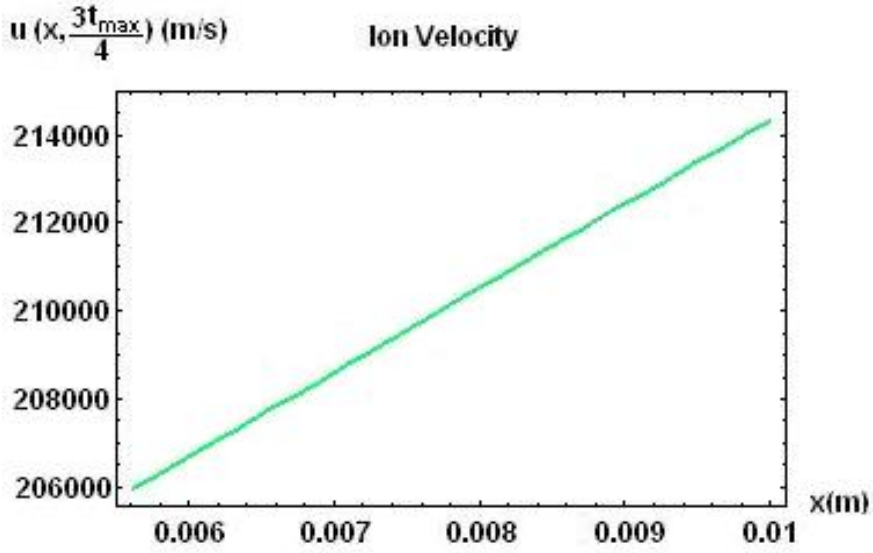

Figure 2.6: Ion velocity as a function of x at time $t = 3t_{\max}/4$.

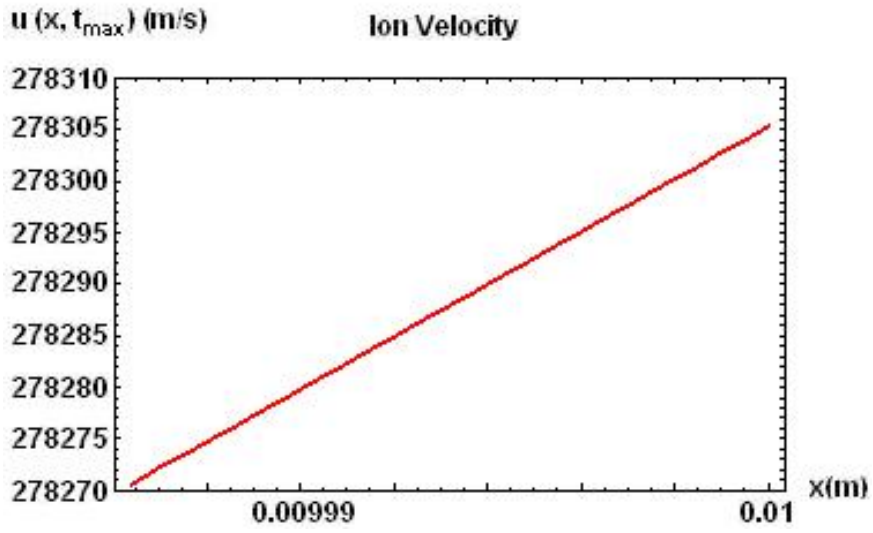

Figure 2.7: Ion velocity as a function of x at time $t = t_{\max}$.

Also, the ion flux is given by equation (2.1.41). Figure 2.8 shows the ion flux as a function of time at $x = L$.

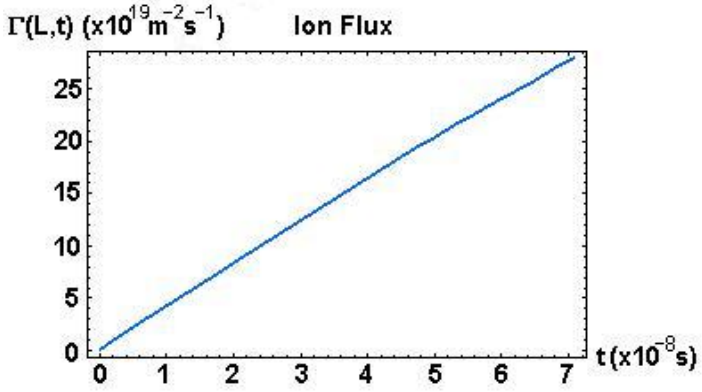

Figure 2.8: Ion flux as a function of t at $x = L$.

2.2. CYLINDRICAL CONFIGURATION

2.2.1. The Model

The problem subject to our work is illustrated in figures 2.9, 2.10 and 2.11, considering the initial phase and the proceeding evolution.

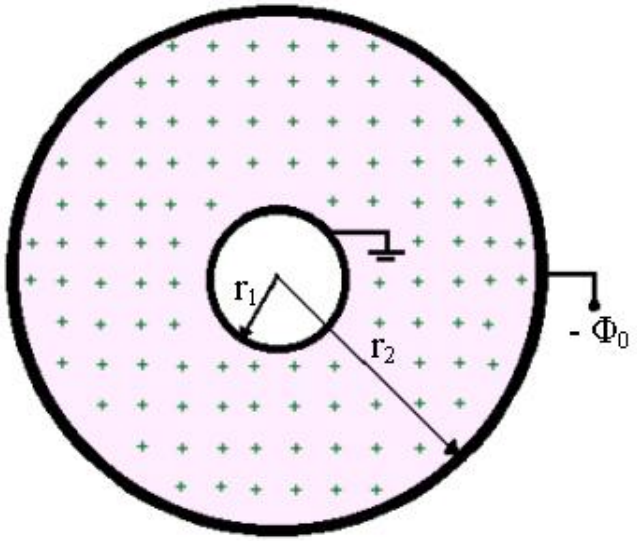

Figure 2.9: When the applied potential, $-\Phi_0$, is large (~ 20 kV) and the electrode separation is small (~ 10^{-2} m), the matrix can fill the entire inter-electrode space ($1/\omega_{pe} < t < 1/\omega_{pi}$), where ω_{pe} and ω_{pi} are electron and ion plasma frequencies, respectively.

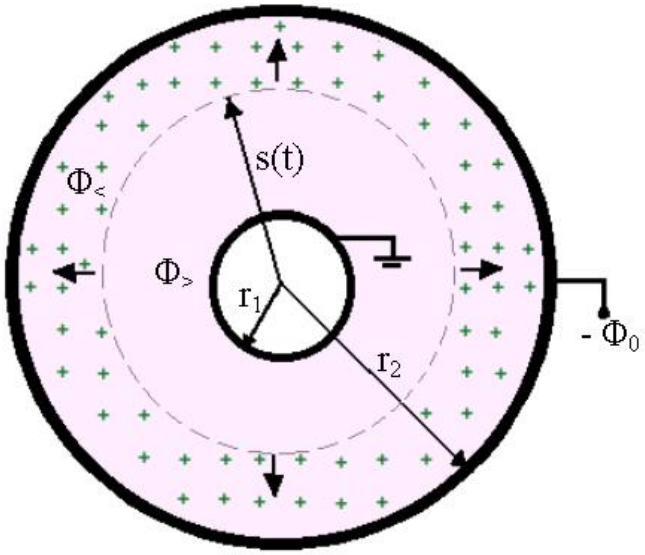

Figure 2.10: After a short time, the matrix starts moving towards the cathode. $s(t)$ is the time-dependent location of the sheath edge.

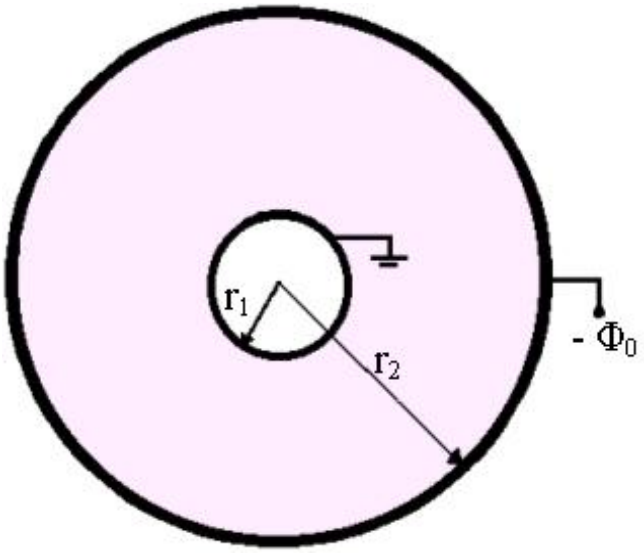

Figure 2.11: The matrix disappears as all ions are implanted.

The model presented here is a one-dimensional model, with a cylindrical anode of infinite length and radius r_1. The target considered is the internal surface of an infinitely long cylinder whose inner radius is r_2. The anode is axially placed inside the target. The magnitude of r_1 is ~ 10^{-2} m, r_2 is ~ 3×10^{-2} m, the negative potential applied to the target, Φ_0, is ~ 20 kV, whereas the anode is kept at zero potential. Potential for $r_1 < r < s(t)$ is labeled as $\Phi_>$ and the potential for $s(t) < r < r_2$ is labeled as $\Phi_<$.

The following assumptions have been made:

1) The ion density n, the potentials $\Phi_<$ and $\Phi_>$, and the ion velocity u_i have a form, which is a zeroth order term that does not take into account the contributions from the ion density plus a first order term due to the contributions from the ion density;

2) Since the contribution of n is already a first order term, any fluctuation in this term is a second order term, and can be neglected in Poisson's Equation;

3) However, both $\Phi_<$ and $\Phi_>$ will be time dependent due to $s(t)$.

Therefore, equations (2.1.1), (2.1.2), (2.1.3) and (2.1.4) are also assumed to be true for the cylindrical case.

2.2.2. The Determination of Potentials

To determine the potentials in both regions $r_1 < r < s(t)$ and $s(t) < r < r_2$, the Poisson's Equations in these regions have to be solved and the boundary conditions have to be imposed.

Since $\Phi_>^{(0)}$ and $\Phi_<^{(0)}$ neglect the effect of n, which is first order, $\Phi_>^{(0)}(r) = \Phi_<^{(0)}(r)$ and the first order potentials $\Phi_>^{(1)}$ and $\Phi_<^{(1)}$ will depend on time.

The Poisson's equations for $\Phi_>^{(0)}$ and $\Phi_<^{(0)}$ are

$$\frac{\partial^2 \Phi_>^{(0)}}{\partial r^2} + \frac{1}{r}\frac{\partial \Phi_>^{(0)}}{\partial r} = \frac{1}{r}\frac{\partial}{\partial r}\left(r\frac{\partial \Phi_>^{(0)}}{\partial r} \right) = 0, \tag{2.2.1}$$

$$\frac{1}{r}\frac{\partial}{\partial r}\left(r\frac{\partial \Phi_<^{(0)}}{\partial r} \right) = 0. \tag{2.2.2}$$

The boundary conditions to be imposed for $\Phi_>^{(0)}$ and $\Phi_<^{(0)}$ are

$$r = r_1, \qquad \Phi_>^{(0)}(r_1) = 0, \tag{2.2.3}$$

$$r = r_2, \qquad \Phi_>^{(0)}(r_2) = \Phi_<^{(0)}(r_2) = -\Phi_0. \tag{2.2.4}$$

Then, the solutions for $\Phi_{>}^{(0)}$ and $\Phi_{<}^{(0)}$ are found as

$$\Phi_{<}^{(0)}(r)=\Phi_{>}^{(0)}(r)=-\Phi_0\frac{\ln(r/r_1)}{\ln(r_2/r_1)}. \tag{2.2.5}$$

The Poisson's equations for $\Phi_{>}^{(1)}$ and $\Phi_{<}^{(1)}$ are

$$\frac{1}{r}\frac{\partial}{\partial r}\left(r\frac{\partial\Phi_{>}^{(1)}}{\partial r}\right)=0, \tag{2.2.6}$$

$$\frac{1}{r}\frac{\partial}{\partial r}\left(r\frac{\partial\Phi_{<}^{(1)}}{\partial r}\right)=-\frac{en}{\varepsilon_0}=-\frac{en_0}{\varepsilon_0}. \tag{2.2.7}$$

The boundary conditions to be imposed for $\Phi_{>}^{(1)}$ and $\Phi_{<}^{(1)}$ are

$$r=r_1, \qquad \Phi_{>}^{(1)}(r_1,t)=0, \tag{2.2.8}$$

$$r=s(t), \qquad \Phi_{>}^{(1)}(r,t)\Big|_{s(t)}=\Phi_{<}^{(1)}(r,t)\Big|_{s(t)}, \tag{2.2.9}$$

$$r=s(t), \qquad \frac{\partial\Phi_{>}^{(1)}}{\partial r}\Big|_{s(t)}=\frac{\partial\Phi_{<}^{(1)}}{\partial r}\Big|_{s(t)}, \tag{2.2.10}$$

$$r=r_2, \qquad \Phi_{<}^{(1)}(r_2,t)=0. \tag{2.2.11}$$

Then, the solutions for $\Phi_{>}^{(1)}$ and $\Phi_{<}^{(1)}$ are found as

$$\Phi_{>}^{(1)}=-\frac{\ln(r/r_1)}{\ln(r_2/r_1)}\left\{\frac{en_0}{4\varepsilon_0}\left[s^2-r_2^2+2s^2\ln(r_2/s)\right]\right\}, \tag{2.2.12}$$

$$\Phi_{<}^{(1)}=-\frac{en_0}{4\varepsilon_0}\left(r^2-r_2^2\right)-\frac{\ln(r/r_2)}{\ln(r_2/r_1)}\left\{\frac{en_0}{4\varepsilon_0}\left[s^2-r_2^2-2s^2\ln(s/r_1)\right]\right\}. \tag{2.2.13}$$

Therefore, the potentials in the regions $r_1 < r < s(t)$ and $s(t) < r < r_2$, i.e. $\Phi_>$ and $\Phi_<$, are found as

$$\Phi_> = -\Phi_0 \frac{\ln(r/r_1)}{\ln(r_2/r_1)} - \frac{\ln(r/r_1)}{\ln(r_2/r_1)} \left\{ \frac{en_0}{4\varepsilon_0} \left[s^2 - r_2^2 + 2s^2 \ln(r_2/s) \right] \right\}, \tag{2.2.14}$$

$$\begin{aligned} \Phi_< = & -\Phi_0 \frac{\ln(r/r_1)}{\ln(r_2/r_1)} - \frac{en_0}{4\varepsilon_0} \left(r^2 - r_2^2 \right) \\ & - \frac{\ln(r/r_2)}{\ln(r_2/r_1)} \left\{ \frac{en_0}{4\varepsilon_0} \left[s^2 - r_2^2 - 2s^2 \ln(s/r_1) \right] \right\} \end{aligned}. \tag{2.2.15}$$

These potentials do not depend on time explicitly. To find the explicit time dependence of the potentials, the explicit form of $s(t)$ must be determined.

To do this, the equation of motion at $r = s(t)$ is used, which is

$$m \frac{d^2 s}{dt^2} = -e \left. \frac{\partial \Phi_>}{\partial r} \right|_{r=s(t)}. \tag{2.2.16}$$

Substituting $\Phi_>$ gives

$$\frac{d^2 s}{dt^2} = \frac{e\Phi_0}{m \ln(r_2/r_1)} \frac{1}{s} \left\{ 1 + \frac{en_0}{4\varepsilon_0 \Phi_0} \left[s^2 - r_2^2 + 2s^2 \ln(r_2/s) \right] \right\}. \tag{2.2.17}$$

To be consistent, $s(t)$ is also assumed to have a form $s(t) = s^{(0)}(t) + s^{(1)}(t)$. Then,

$$\begin{aligned} \frac{d^2 s}{dt^2} &= \frac{d^2 s^{(0)}}{dt^2} + \frac{d^2 s^{(1)}}{dt^2} \\ &= \frac{e\Phi_0}{m \ln(r_2/r_1)} \frac{1}{s} \left\{ 1 + \frac{en_0}{4\varepsilon_0 \Phi_0} \left[s^2 - r_2^2 + 2s^2 \ln(r_2/s) \right] \right\} \end{aligned}. \tag{2.2.18}$$

In $s(t)$, the first order term is much smaller than the zeroth order term. Then, $\frac{1}{s}$ and s^2 can be expanded as given by equations (2.2.19) and (2.2.20).

$$\frac{1}{s} = \frac{1}{s^{(0)} + s^{(1)}} = \frac{1}{s^{(0)}}\left[1 + \frac{s^{(1)}}{s^{(0)}}\right]^{-1} = \frac{1}{s^{(0)}}\left[1 - \frac{s^{(1)}}{s^{(0)}}\right], \tag{2.2.19}$$

$$s^2 = \left(s^{(0)}\right)^2\left[1 - \frac{s^{(1)}}{s^{(0)}}\right]^{-2} = \left(s^{(0)}\right)^2\left[1 + \frac{2s^{(1)}}{s^{(0)}}\right]. \tag{2.2.20}$$

Then, the equation of motion at $r = s(t)$ becomes

$$\frac{d^2 s^{(0)}}{dt^2} + \frac{d^2 s^{(1)}}{dt^2} = \frac{e\Phi_0}{m\ln(r_2/r_1)s^{(0)}}\left\{\begin{array}{l}\left(1 - \frac{s^{(1)}}{s^{(0)}}\right) + \\ \frac{en_0\left(s^{(0)}\right)^2}{4\varepsilon_0\Phi_0}\left(1 + \frac{2s^{(1)}}{s^{(0)}}\right)\left[1 - \frac{\left(r_2/s^{(0)}\right)^2}{\left(1 + \frac{2s^{(1)}}{s^{(0)}}\right)^2} + 2\ln\left(\frac{r_2}{s^{(0)}}\left[1 - \frac{s^{(1)}}{s^{(0)}}\right]\right)\right]\end{array}\right\} \tag{2.2.21}$$

Note that $\left[\frac{en_0\left(s^{(0)}\right)^2}{4\varepsilon_0\Phi_0}\right]_{\max} = \frac{en_0 r_2^2}{4\varepsilon_0\Phi_0}$, which is a first order term.

Then, omitting the second order terms in equation (2.2.21) equation (2.2.2) is obtained.

$$\frac{d^2 s^{(0)}}{dt^2} + \frac{d^2 s^{(1)}}{dt^2} = \frac{e\Phi_0}{m\ln(r_2/r_1)s^{(0)}}\left\{\begin{array}{l}1 - \frac{s^{(1)}}{s^{(0)}} \\ + \frac{en_0\left(s^{(0)}\right)^2}{4\varepsilon_0\Phi_0}\left[1 - \left(\frac{r_2}{s^{(0)}}\right)^2 + 2\ln\left(\frac{r_2}{s^{(0)}}\right)\right]\end{array}\right\} \tag{2.2.22}$$

Since $\frac{s^{(1)}}{s^{(0)}}$ and $\left[\frac{en_0 s^{(0)^2}}{4\varepsilon_0\Phi_0}\right]_{\max} = \frac{en_0 r_2^2}{4\varepsilon_0\Phi_0}$ are first order terms, the differential equation of $s^{(0)}(t)$ is

$$\frac{d^2 s^{(0)}}{dt^2} = \frac{e\Phi_0}{m\ln(r_2/r_1)}\frac{1}{s^{(0)}}. \tag{2.2.23}$$

The differential equation of $s^{(1)}(t)$ is

$$\frac{d^2 s^{(1)}}{dt^2} = \frac{e\Phi_0}{ms^{(0)}\ln(r_2/r_1)}\left\{-\frac{s^{(1)}}{s^{(0)}} + \frac{en_0\left(s^{(0)}\right)^2}{4\varepsilon_0\Phi_0}\left[1-\left(\frac{r_2}{s^{(0)}}\right)^2 + 2\ln\left(\frac{r_2}{s^{(0)}}\right)\right]\right\}. \tag{2.2.24}$$

Therefore, from the differential equations (2.2.23), to find $s^{(0)}(t)$ let $\frac{ds^{(0)}}{dt} = p$, then

$$\frac{d^2 s^{(0)}}{dt^2} = \frac{1}{2}\frac{d\left(p^2\right)}{ds^{(0)}} = \frac{e\Phi_0}{m\ln(r_2/r_1)}\frac{1}{s^{(0)}} \tag{2.2.25}$$

which can be separated as

$$d\left(p^2\right) = \frac{2e\Phi_0}{m\ln(r_2/r_1)}\frac{ds^{(0)}}{s^{(0)}} \tag{2.2.26}$$

Hence, integrating both sides equation (2.2.27) is obtained.

$$p^2 = \left(\frac{ds^{(0)}}{dt}\right)^2 = \frac{2e\Phi_0}{m\ln(r_2/r_1)}\ln s^{(0)} + C. \tag{2.2.27}$$

The initial conditions to be imposed for $s^{(0)}$ and $\frac{ds^{(0)}}{dt}$ are

$$t = 0, \qquad p(t=0) = \left.\frac{ds^{(0)}}{dt}\right|_{t=0} = 0 \tag{2.2.28}$$

$$t = 0, \qquad s^{(0)}(t=0) = r_1 . \tag{2.2.29}$$

Then, the following results are found.

$$C = -\frac{2e\Phi_0}{m\ln(r_2/r_1)}\ln r_1 \tag{2.2.30}$$

$$\frac{ds^{(0)}}{dt} = \left[\frac{2e\Phi_0}{m\ln(r_2/r_1)}\ln\left(s^{(0)}/r_1\right)\right]^{1/2} \tag{2.2.31}$$

To simplify the equation, the following definitions are made

$$a = \left[\frac{2e\Phi_0}{mr_1^2\ln(r_2/r_1)}\right]^{1/2} = 2.696\times10^7\, s^{-1} \tag{2.2.32}$$

$$x = \left(s^{(0)}/r_1\right). \tag{2.2.33}$$

Then, the differential equation (2.2.31) takes the form

$$\frac{d(x)}{dt} = a\left[\ln(x)\right]^{1/2} \tag{2.2.34}$$

which is given in equation (2.2.35) in integral form.

$$a\,t = \int_1^x \frac{dx'}{\left[\ln x'\right]^{1/2}} \tag{2.2.35}$$

To find the solution of this integral, assumption

$$\frac{1}{\left[\ln x'\right]^{1/2}} \cong \frac{1}{\left[x'-1\right]^{1/2}} + 0.15\left[x'-1\right] \text{ for } 1 \le x \le 3, \tag{2.2.36}$$

is made with a maximum error of 4%.

Then, the integral equation becomes

$$a\,t = \int_1^x \left\{ \frac{1}{\left[x'-1\right]^{1/2}} + 0.15\left[x'-1\right] \right\} dx' \text{ for } 1 \le x \le 3. \tag{2.2.37}$$

Defining $u = \left[x'-1\right]^{1/2}$, $du = \frac{1}{2\left[x'-1\right]^{1/2}} dx'$, the solution is found as

$$a\,t = 2u + 0.3\frac{u^4}{4} \tag{2.2.38}$$

which can be written as

$$u^4 + 26.6u - 13.3at = 0. \tag{2.2.39}$$

Note that $\left[u\right]_{\max} \cong 1.4$ and $\left[u^4\right]_{\max} \cong \left(1.4\right)^4 = 3.84$ which is very small compared to $\left[26.6u\right]_{\max} \cong 37.2$. So it can be ignored. Then,

$$u \cong \frac{at}{2}. \tag{2.2.40}$$

To get a better result u is defined as

$$u = u_0(1+\delta) \tag{2.2.41}$$

where

$$u_0 \cong \frac{at}{2} \tag{2.2.42}$$

$$\delta << 1. \tag{2.2.43}$$

Substituting these values into equation (2.2.39) and using the fact that $[u]_{\max} \cong \left[\frac{at}{2}\right]_{\max} \cong 1.4$ and $4\left(\frac{at}{2}\right)^4 << 26.6\left(\frac{at}{2}\right)$, δ is found as

$$\delta \cong -\frac{(at/2)^3}{26.6} << 1 \tag{2.2.44}$$

Then, u is found as

$$u = u_0(1+\delta) = (at/2)\left[1 - \frac{(at/2)^3}{26.6}\right] \tag{2.2.45}$$

Since $u = (x-1)^{1/2}$, x is found as

$$x = (at/2)^2\left[1 - \frac{(at/2)^3}{26.6}\right]^2 + 1 = (at/2)^2 - \frac{(at/2)^5}{13.3} + 1 \tag{2.2.46}$$

Again using the fact that $\frac{(at/2)^5}{13.3} << 1$,

$$x \cong 1 + (at/2)^2 . \tag{2.2.47}$$

Remember that $x = \left(s^{(0)}/r_1\right)$. Therefore $s^{(0)}$ is found as

$$s^{(0)}(t) \cong r_1\left[1 + (at/2)^2\right] \tag{2.2.48}$$

where a is defined by the equation (2.2.32).

To find $s^{(1)}$, $s^{(0)}$ is substituted into equation (2.2.24).

$$\begin{aligned}\frac{d^2 s^{(1)}}{dt^2} = &-\frac{e\Phi_0}{m r_1^{\,2} \ln(r_2/r_1)} \frac{s^{(1)}}{\left[1 + (at/2)^2\right]^2} \\ &+ \frac{e^2 n_0 r_1 \left[1 + (at/2)^2\right]}{4\varepsilon_0 m \ln(r_2/r_1)} \left\{1 - \frac{(r_2/r_1)^2}{\left[1 + (at/2)^2\right]^2} + 2\ln(r_2/r_1) - 2\ln\left[1 + (at/2)^2\right]\right\}\end{aligned} \tag{2.2.49}$$

To simplify this equation, the change of variables $\omega = (at/2)$ is made.

$$\frac{d^2 s^{(1)}}{d\omega^2} + \frac{2s^{(1)}}{\left[1 + \omega^2\right]^2} = \frac{e n_0 r_1^{\,3}\left[1 + \omega^2\right]}{2\varepsilon_0 \Phi_0} \left\{1 - \frac{(r_2/r_1)^2}{\left[1 + \omega^2\right]^2} + 2\ln\left(\frac{r_2}{r_1}\right) - 2\ln\left[1 + \omega^2\right]\right\} \tag{2.2.50}$$

This equation can be solved using variation of parameters but this is not necessary.

Dividing expressions for $\Phi_>^{(1)}$ and $\Phi_<^{(1)}$ by $\Phi^{(0)}$ gives first order terms on the left hand side.

$$\frac{\Phi_{>}^{(1)}}{\Phi^{(0)}} = \left\{ \frac{en_0 s^2}{4\varepsilon_0 \Phi_0} \left[1 - \left(r_2 / s \right)^2 + 2\ln\left(r_2 / s \right) \right] \right\}$$

$$\frac{\Phi_{<}^{(1)}}{\Phi^{(0)}} - \frac{\dfrac{en_0}{4\varepsilon_0}\left(r^2 - r_2^2 \right)}{\Phi_0 \dfrac{\ln\left(r/r_1 \right)}{\ln\left(r_2/r_1 \right)}} = \frac{\ln\left(r/r_2 \right)}{\ln\left(r/r_1 \right)} \left\{ \frac{en_0 s^2}{4\varepsilon_0 \Phi_0} \left[1 - \left(r_2 / s \right)^2 - 2\ln\left(s/r_1 \right) \right] \right\} \tag{2.2.51}$$

Since $\left[\dfrac{en_0 \left(s^{(0)} \right)^2}{4\varepsilon_0 \Phi_0} \right]_{\max} = \dfrac{en_0 r_2^2}{4\varepsilon_0 \Phi_0}$ is a first order term, for the terms on the right hand side not to be second order terms, only $\left(s^{(0)} \right)^2$ is needed as $\dfrac{en_0}{4\varepsilon_0 \Phi_0}\left(2 s^{(0)} s^{(1)} \right)$ will be of second order. Also for this reason, the approximation of $s^{(0)}$ given by equation (2.2.48) can be made.

Then, the explicit forms of the potentials $\Phi_{>}$ and $\Phi_{<}$ are given by

$$\begin{aligned} \Phi_{>} = & -\frac{\ln\left(r/r_1 \right)}{\ln\left(r_2/r_1 \right)} \Phi_0 \\ & - \frac{\ln\left(r/r_1 \right)}{\ln\left(r_2/r_1 \right)} \frac{en_0 r_1^2 \left[1 + \left(\frac{at}{2} \right)^2 \right]^2}{4\varepsilon_0} \left[1 - \frac{\left(r_2/r_1 \right)^2}{\left[1 + \left(\frac{at}{2} \right)^2 \right]^2} + 2\ln\left(\frac{r_2}{r_1} \right) - 2\ln\left[1 + \left(\frac{at}{2} \right)^2 \right] \right] \end{aligned} \tag{2.2.52}$$

$$\begin{aligned} \Phi_{<} = & -\Phi_0 \frac{\ln\left(r/r_1 \right)}{\ln\left(r_2/r_1 \right)} \\ & - \frac{\ln\left(r/r_2 \right)}{\ln\left(r_2/r_1 \right)} \frac{en_0 r_1^2 \left[1 + \left(\frac{at}{2} \right)^2 \right]^2}{4\varepsilon_0} \left[1 - \frac{\left(r_2/r_1 \right)^2}{\left[1 + \left(\frac{at}{2} \right)^2 \right]^2} - 2\ln\left[1 + \left(\frac{at}{2} \right)^2 \right] \right] \\ & - \frac{en_0}{4\varepsilon_0}\left(r^2 - r_2^2 \right) \end{aligned} \tag{2.2.53}$$

2.2.3. The Determination of Ion Velocity and Flux

To examine the ion behavior, the ion velocity and the flux must be determined. To do this, the equation of motion is considered.

$$\frac{du_i}{dt} = \frac{\partial u_i}{\partial t} + u_i \frac{\partial u_i}{\partial r} = -\frac{e}{m}\frac{\partial \Phi_<}{\partial r}. \tag{2.2.54}$$

Substituting $\frac{\partial \Phi_<}{\partial r}$, equation (2.2.54) takes the form

$$\begin{aligned}\frac{du_i}{dt} &= \frac{\partial u_i}{\partial t} + u_i \frac{\partial u_i}{\partial r} \\ &= \frac{e\Phi_0}{m\ln(r_2/r_1)}\frac{1}{r}\left\{1 + \frac{en_0 r_1^{\,2}\left[1+\left(\frac{at}{2}\right)^2\right]^2}{4\varepsilon_0\Phi_0}\left[1 - \frac{(r_2/r_1)^2}{\left[1+\left(\frac{at}{2}\right)^2\right]^2} - 2\ln\left[1+\left(\frac{at}{2}\right)^2\right]\right]\right\} \\ &\quad + \frac{e^2 n_0}{2\varepsilon_0 m} r\end{aligned} \tag{2.2.55}$$

Using the assumption given by equation (2.1.4), two differential equations for the zeroth order ion velocity and for the first order ion velocity are obtained.

$$\frac{\partial u_i^{(0)}}{\partial t} + u_i^{(0)}\frac{\partial u_i^{(0)}}{\partial r} = \frac{e\Phi_0}{m\ln(r_2/r_1)}\frac{1}{r} \tag{2.2.56}$$

$$\frac{\partial u_i^{(1)}}{\partial t} + u_i^{(0)}\frac{\partial u_i^{(1)}}{\partial r} + u_i^{(1)}\frac{\partial u_i^{(0)}}{\partial r} = \frac{e^2 n_0 r_1^{\,2}\left[1+\left(\frac{at}{2}\right)^2\right]^2}{4\varepsilon_0 m\ln(r_2/r_1) r}\left[1 - \frac{(r_2/r_1)^2}{\left[1+\left(\frac{at}{2}\right)^2\right]^2} - 2\ln\left[1+\left(\frac{at}{2}\right)^2\right]\right] + \frac{e^2 n_0}{2\varepsilon_0 m} r \tag{2.2.57}$$

Equation (2.2.56) is a quasi-linear partial differential equation and can be solved by the method of characteristics, i.e. by solving the ordinary differential equations given by equation (2.2.58).

$$\frac{dt}{1} = \frac{dr}{u_i^{(0)}} = \frac{du_i^{(0)}}{\dfrac{e\Phi_0}{m\ln\left(r_2/r_1\right)}\dfrac{1}{r}} \tag{2.2.58}$$

The differential equation

$$\frac{dr}{u_i^{(0)}} = \frac{du_i^{(0)}}{\dfrac{e\Phi_0}{m\ln\left(r_2/r_1\right)}\dfrac{1}{r}} \tag{2.2.59}$$

has a solution in the form

$$u_i^{(0)} = ar_1\left[\ln\left(r/r_0\right)\right]^{1/2} \tag{2.2.60}$$

where r_0 denotes the initial position at $t = 0$, which can be any point in the interval $r_1 \le r \le r_2$, and a is given by equation (2.2.32).

Using $u_i^{(0)}$ given by equation (2.2.60), the differential equation

$$\frac{dt}{1} = \frac{dr}{u_i^{(0)}} \tag{2.2.61}$$

can be written in integral form as

$$\int_0^t \frac{ar_1}{r_0}dt = \int_1^{r/r_0} \frac{d\left(r/r_0\right)}{\left[\ln\left(r/r_0\right)\right]^{1/2}}. \tag{2.2.62}$$

With the simplification $x = r/r_0$, the integral in equation (2.2.62) becomes

$$\frac{ar_1}{r_0}t = \int_1^x \frac{dx'}{\sqrt{\ln x'}}\,. \tag{2.2.63}$$

The solution of equation (2.2.63) is found to be

$$\frac{ar_1}{r_0}t = -i\sqrt{\pi}\,Erf\left(i\sqrt{\ln x}\right). \tag{2.2.64}$$

Figure 2.12 shows the graph of $-i\sqrt{\pi}\,Erf\left(i\sqrt{\ln x}\right)$ and figure 2.13 shows the graph of the solution given by equation (2.2.64).

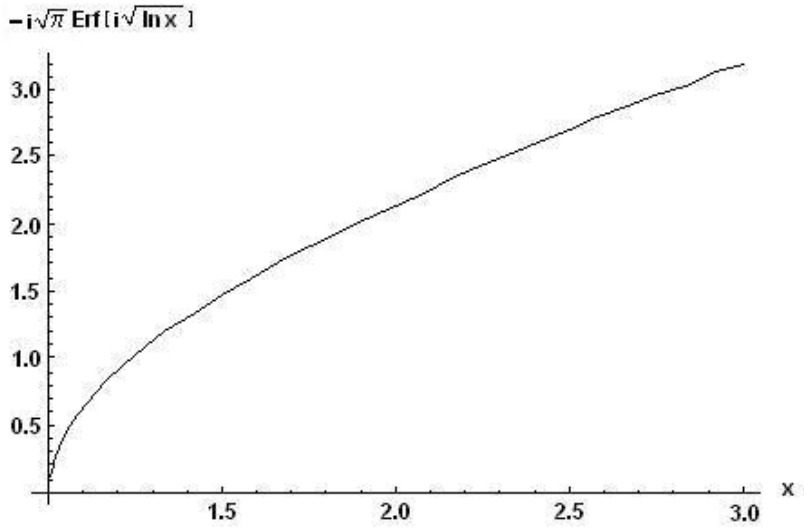

Figure 2.12: The graph of $-i\sqrt{\pi}\,Erf\left(i\sqrt{\ln x}\right)$ where $x = r/r_0$.

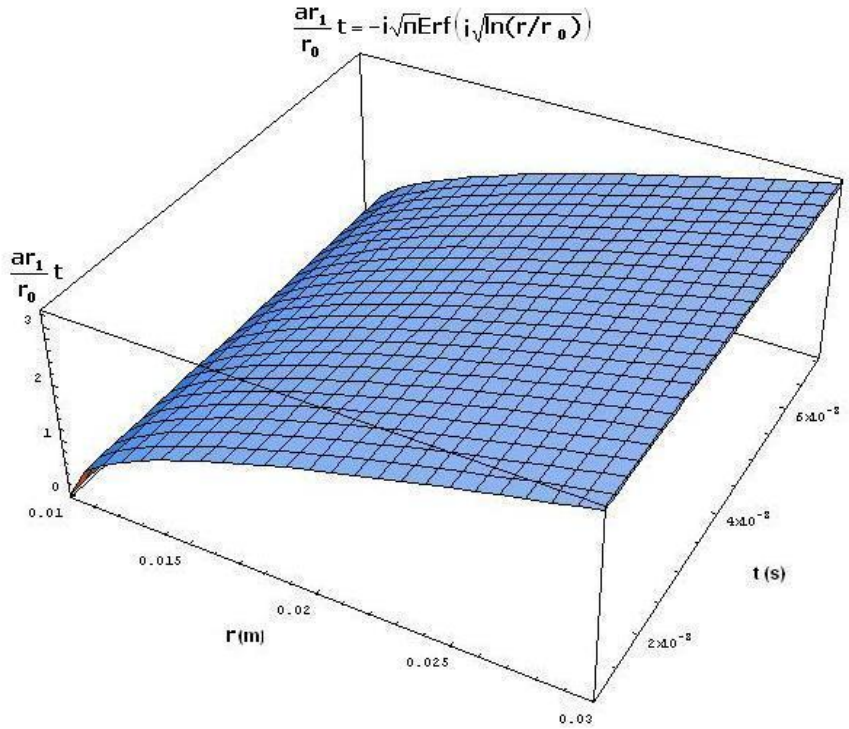

Figure 2.13: The graph of $\frac{ar_1}{r_0}t = -i\sqrt{\pi}Erf\left(i\sqrt{\ln(r/r_0)}\right)$ with r_0 taken as $r_0 = r_1$.

The solution given by (2.2.64) cannot be used in this form since it is imaginary. When $-i\sqrt{\pi}Erf\left(i\sqrt{\ln(r/r_0)}\right)$ is written in the infinite series form, equation (2.2.65), it is observed that the solution is real.

$$-i\sqrt{\pi}Erf\left(i\sqrt{\ln(r/r_0)}\right) = 2\sum_{n=0}^{\infty}\frac{\left[\sqrt{\ln(r/r_0)}\right]^{2n+1}}{n!(2n+1)} \qquad (2.2.65)$$

Using the fact that r/r_0 can take values in the interval $0 \le r/r_0 \le 3$, $\sqrt{\ln(r/r_0)}$ can take values in the interval $0 \le \sqrt{\ln(r/r_0)} \le 1.048$. The maximum value of $\sqrt{\ln(r/r_0)}$ is used to compare the first five terms ($0 \le n \le 4$) in the infinite series

given by equation (2.2.65). These five terms correspond to 1, 0.37, 0.12, 0.03 and 0.007, respectively. Then, the first three terms ($n = 0,1,2$) can be considered of equal orders and the other terms can be excluded. However, it is not possible to solve equation (2.2.65) analytically after this approximation unless the third term is also excluded. Then, equation (2.2.65) can be written in the form given by equation (2.2.66) where only the first two terms in the expansion are taken with an error of 9 %. The solution of equation (2.2.64) is given by (2.2.67).

$$-i\sqrt{\pi}Erf\left(i\sqrt{\ln(r/r_0)}\right) = 2\sqrt{\ln(r/r_0)} + \frac{2}{3}\left[\sqrt{\ln(r/r_0)}\right]^3 \qquad (2.2.66)$$

$$\frac{ar_1}{r_0}t = 2\sqrt{\ln(r/r_0)} + \frac{2}{3}\left[\sqrt{\ln(r/r_0)}\right]^3. \qquad (2.2.67)$$

When the graphs of equation (2.2.64) and (2.2.67) are plotted for $t = t_{\max}$ and $r_0 = r_1$, the difference in solutions can be seen in figure 2.14.

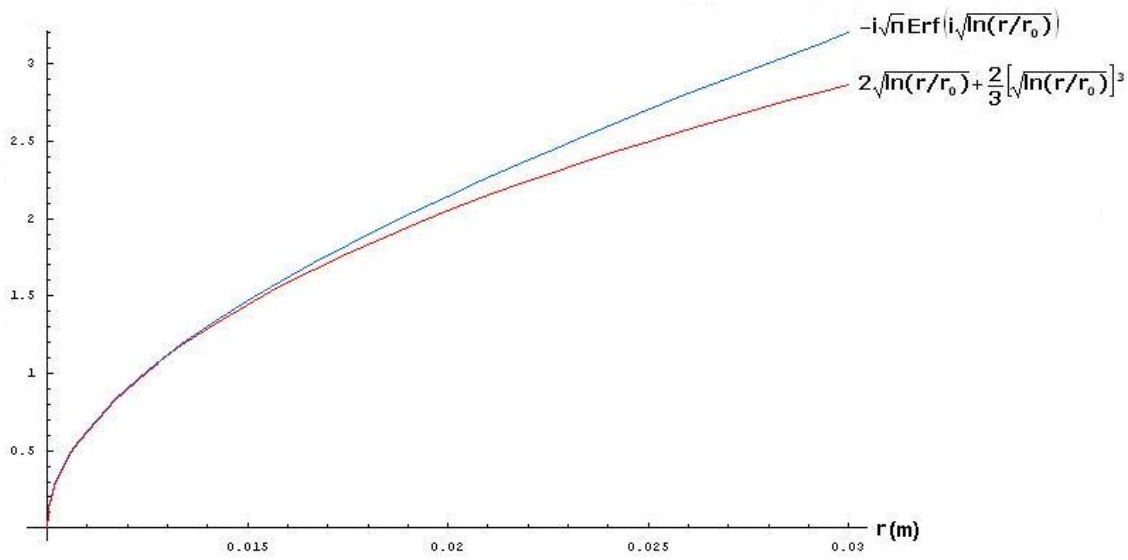

Figure 2.14: A comparison of the graphs of equation (2.2.64) and (2.2.67) for $t = t_{\max}$ and $r_0 = r_1$.

Equation (2.2.67) is solved for $r(t)$ by using the mathematical packet program Mathematica and thus three roots are obtained. The only real root is given in equation (2.2.68).

$$r(t) = r_0 e^{f(t)} \tag{2.2.68}$$

where

$$f(t) = -2 + \frac{3.78}{\left(54 + \frac{4.42\times10^{12}\times t^2}{r_0^{\,2}} + \sqrt{-2916 + \left(54 + \frac{4.42\times10^{12}\times t^2}{r_0^{\,2}}\right)^2}\right)^{1/3}} + 0.265\left(54 + \frac{4.42\times10^{12}\times t^2}{r_0^{\,2}} + \sqrt{-2916 + \left(54 + \frac{4.42\times10^{12}\times t^2}{r_0^{\,2}}\right)^2}\right)^{1/3} \tag{2.2.69}$$

When equation (2.2.68) is taken as the solution for $r(t)$ and this solution is substituted into the equation (2.2.60), equation (2.2.70) is obtained.

$$u_i^{(0)} = a r_1 \left[f(t)\right]^{1/2} \tag{2.2.70}$$

It can be easily seen that this solution method has lead to a solution for the zeroth order ion velocity with the form $u_i^{(0)} = u_i^{(0)}(t)$. However, simulations have shown that the zeroth order ion velocity has the form $u_i^{(0)}(r,t)$. Since solving equation (2.2.67) for $r_0(r,t)$, which may lead to a solution of the form $u_i^{(0)}(r,t)$, is not analytically possible, it can be concluded that expressing of the imaginary error function in infinite series form will not give an acceptable solution.

To find an acceptable solution for the zeroth order ion velocity, the fact that equation (2.2.63) has the same form with equation (2.2.35) is taken into account. Then, doing similar calculations, (r/r_0) is found as

$$(r/r_0)=\left(\frac{ar_1}{2r_0}\right)^2 t^2+1,\ 1\le(r/r_0)\le 3 \qquad (2.2.71)$$

where a is given by equation (2.2.32). Equation (2.2.71) can be written in quadratic form as

$$r_0{}^2-rr_0+\frac{a^2r_1{}^2}{4}t^2=0 \qquad (2.2.72)$$

This quadratic equation has two roots in the following form

$$(r_0)_{1,2}=\frac{r\pm\sqrt{r^2-a^2r_1{}^2t^2}}{2} \qquad (2.2.73)$$

To find the root that is valid, the graph of $r_0(r-r_0)$, which is shown in figure 2.15, is plotted and examined. Note that the graph in figure 2.15 actually belongs to $r_0(r-r_0)=\frac{a^2r_1{}^2}{4}t^2$.

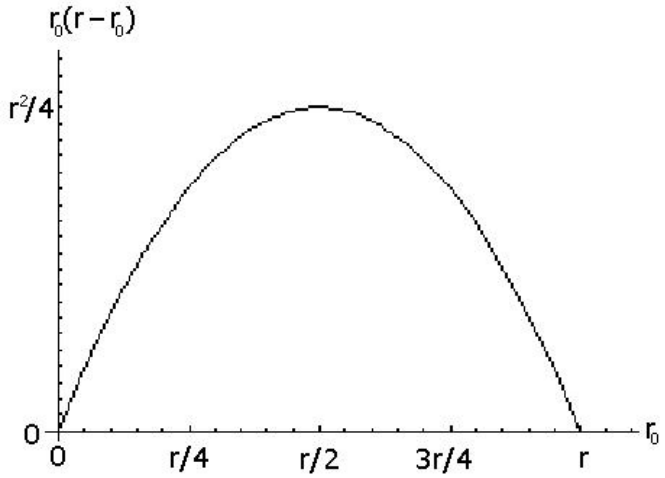

Figure 2.15: The graph of $r_0(r-r_0)$.

From the graph it is easily seen that both roots of r_0 are valid solutions. The negative root corresponds to the region $0 \le r_0 \le r/2$ and the positive root corresponds to the region $r/2 \le r_0 \le r$. In our model $r = r_2$ and the regions where roots correspond are shown in figure 2.16.

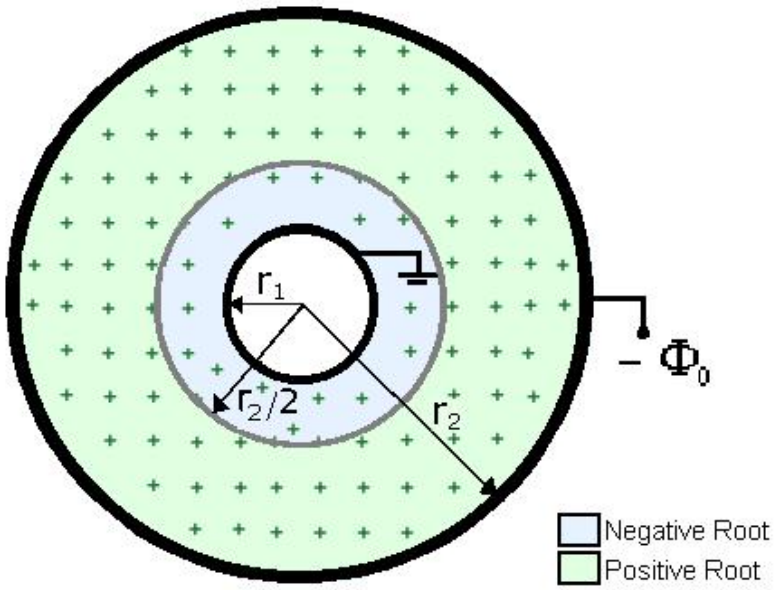

Figure 2.16: The regions where the roots of r_0 correspond.

Substituting the roots of r_0 into equation (2.2.60) and using the approximation given by equation (2.2.36), $u_i^{(0)}$ is found

$$u_i^{(0)} = \begin{cases} \dfrac{ar_1 z^2}{ar_1\left[r-\sqrt{r^2-z^2}\right]+0.3\left[r^2+r\sqrt{r^2-z^2}-\frac{1}{2}z^2\right]}, & r_1 \le r \le r_2/2 \\ \dfrac{ar_1 z^2}{ar_1\left[r+\sqrt{r^2-z^2}\right]+0.3\left[r^2-r\sqrt{r^2-z^2}-\frac{1}{2}z^2\right]}, & r_2/2 \le r \le r_2 \end{cases} \qquad (2.2.74)$$

where $z = ar_1 t$ and a is defined by the equation (2.2.32). However, equation (2.2.74), which is obtained analytically under the approximation (2.2.36), needs to be studied further because it does not fully satisfy equation (2.2.56).

Solving equation (2.2.56) and (2.2.57) by using numeric methods, the ion velocity, $u_i = u_i^{(0)} + u_i^{(1)}$, was obtained as shown in figure 2.17. In the numerical calculations, the ions are assumed to be titanium ions and the ion mass is taken to be $48 \times 1.67 \times 10^{-27}$ kg, the radius of anode, r_1, is taken to be ~10^{-2} m, the inner radius of cathode, r_2, is taken to be ~3×10^{-2} m, the magnitude of the distance between the electrodes, L, is taken to be ~2×10^{-2} m, the negative potential applied to the cathode, Φ_0, is taken to be ~ 20 kV, potential applied to the anode is taken to be 0.0 kV, the initial ion velocity is taken to be 0.0 m/s and the initial ion density, n_0, is taken to be ~ 10^{15} /m^3.

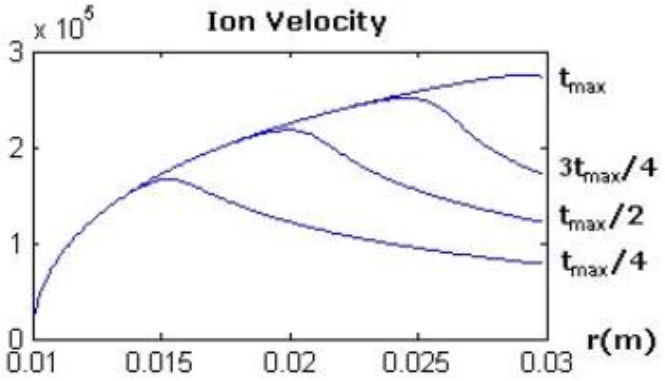

Figure 2.17: The ion velocity as a function of r at the instants $t = \frac{t_{\max}}{4}$, $t = \frac{t_{\max}}{2}$, $t = \frac{3t_{\max}}{4}$ and $t = t_{\max}$ obtained as a result of numeric calculations.

Then, the ion flux on the surface of the target as a function of time is found numerically. Figure 2.18 shows the graph of the ion flux obtained as a result of these numeric calculations.

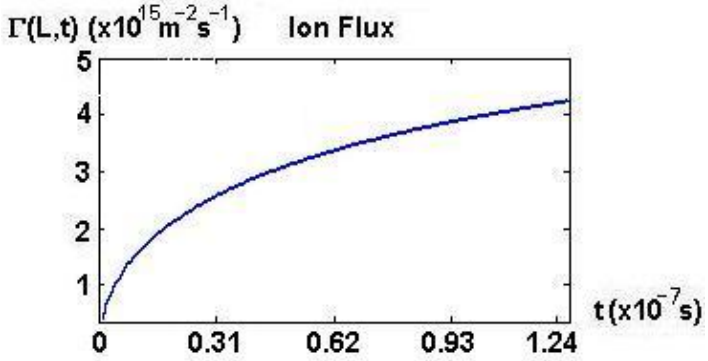

Figure 2.18: The ion flux as a function of t at the target surface obtained as a result of numeric calculations.

CHAPTER 3

SIMULATION

3.1. THE BASICS OF SIMULATION

3.1.1. Numerical Analysis

Many problems in mathematics do not have a solution in closed form. In these situations, an approximate solution using asymptotic analysis or a numerical solution is sought. The numerical analysis is the study of algorithms for the problems of continuous mathematics using basic arithmetical operations [19].

In numerical analysis, the algorithms that can solve a problem exactly are called direct methods; the algorithms that solve the problem by successive approximations are called iterative methods. The process of replacing a continuous problem with a discrete problem whose solution is approximately equal to that of the continuous problem is called discretization.

Numerical analysis is concerned with computing the solution of both ordinary differential equations and partial differential equations in its application areas, which include computational physics, computational fluid dynamics, weather forecasting, climate models, the analysis and design of molecules (computational chemistry) and economy.

Partial differential equations are solved by first discretizing the equation. Three common methods of discretization of partial differential equations are the finite element method, the finite volume method and the finite-differences method.

3.1.2. The Finite-Differences Method

The finite-differences method is a numerical method for solving partial and ordinary differential equations, which aims to replace the continuous derivatives with difference equations that involve only the discrete values of the unknown function related to the position in the domain of the problem [20].

The finite-differences method discretizes the domain of the problem into a regular grid (mesh) defined by a certain number of nodes which are separated in the direction of coordinates by a certain spatial and time interval. For a problem solved with the explicit finite-differences method to converge to the exact solution, the time step must be smaller than a certain maximal value [21]. For example, the stable explicit differencing schemes for solving the advection equation are subject to the Courant-Friedrichs-Levy (CFL) condition, which determines the maximum allowable time step [22]. The CFL condition, which gives the condition of the convergence of a difference approximation in terms of the concept of domain dependence, states that for a convergent algorithm, the domain of dependence of the partial differential equation must lie within the domain of dependence of the numerical algorithm. This, in turn implies a condition on the time step, given by equation (3.1.1) [23].

The CFL condition on the time step:

$$\delta t \leq \frac{\delta x}{v} \tag{3.1.1}$$

where v is a phase speed or an advection velocity and $v > 0$.

On the other hand, for a problem solved with the implicit finite-differences method, there is no stability requirement on the time step; the value of the time step is dictated by accuracy only.

When the finite-differences method is applied over the mesh, the unknown function is approximated at each one of the nodes, giving a difference equation that relates the value of the function at a particular node with its value at the neighboring nodes [24]. This procedure is repeated at each node composing the grid resulting in a system of difference equations which may be numerically solved either with iterative approximate methods or with direct decomposition methods.

The discretization of one-dimensional partial differential equations usually leads to standard three-point problems (also known as tridiagonal equation systems) [25 – 26] which may be written as

$$\begin{cases} b_1 U_1 - c_1 U_2 = d_1, \\ -a_j U_{j-1} + b_j U_j - c_j U_{j+1} = d_j, \quad j = 2,..,n-1,. \\ -a_n U_{n-1} + b_n U_n = d_n. \end{cases} \tag{3.1.2}$$

In three-point problems, the equation number j involves only the terms with numbers $j-1$, j and $j+1$ so that the matrix of the system has non-zero elements only on the diagonal and in the positions immediately to the left and right of the diagonal as shown in equation (3.1.3) [26].

$$\begin{bmatrix} b_1 & c_1 & . & . & 0 \\ a_2 & b_2 & c_2 & . & . \\ . & a_3 & b_3 & . & . \\ . & . & . & . & c_{n-1} \\ 0 & . & . & a_n & b_n \end{bmatrix} \begin{bmatrix} U_1 \\ U_2 \\ . \\ . \\ U_n \end{bmatrix} = \begin{bmatrix} d_1 \\ d_2 \\ . \\ . \\ d_n \end{bmatrix} \tag{3.1.3}$$

To solve three-point problems, tridiagonal matrix algorithms such as the Thomas algorithm are used.

The Thomas algorithm, which is a direct method, requires the known coefficients a_j, b_j and c_j to satisfy the conditions given by equations (3.1.4) and (3.1.5),

which ensure that the matrix form of the three-point problem is diagonally dominant [26].

$$a_j > 0,\ b_j > 0,\ c_j > 0 \tag{3.1.4}$$

$$b_j > a_j + c_j \tag{3.1.5}$$

The Thomas algorithm solves the three-point problem by reducing the system of equations to upper triangular form, by eliminating the term U_{j-1} in each equation turning them into a new form given by equation (3.1.6) [26].

$$U_j - e_j U_{j+1} = f_j,\ \ j = 1,2,...,n-1 \tag{3.1.6}$$

where e_j and f_j satisfy the recurrence relations given by equations (3.1.7) and (3.1.8) and have initial values given by equation (3.1.9) [26].

$$e_j = \frac{c_j}{b_j - a_j e_{j-1}},\ \ j = 1,2,...,n \tag{3.1.7}$$

$$f_j = \frac{d_j + a_j f_{j-1}}{b_j - a_j e_{j-1}},\ \ j = 1,2,...,n \tag{3.1.8}$$

$$e_0 = \frac{c_1}{b_1} \text{ and } f_0 = \frac{d_1}{b_1}. \tag{3.1.9}$$

After finding the coefficients by using the recurrence relations given by equations (3.1.7) and (3.1.8), the values of U_j are easily calculated using equation (3.1.6).

For stability, the condition each $|e_j| < 1$ in equation (3.1.6) must hold, which is already guaranteed by the equations (3.1.4) and (3.1.5).

3.2. PLANAR CONFIGURATION

3.2.1. The Model

The model presented in the planar part of our problem is a one-dimensional model, with a planar anode of infinite area placed at $x = 0$ and a planar cathode at $x = L$ where the target to be implanted is placed. The target considered is also a planar plate that has an infinite area. The magnitude of L is ~ 10^{-2} m, and the negative potential applied to the cathode, Φ_0, is ~ 20 kV, whereas the anode is kept at zero potential, the ion velocity is initially zero and the initial ion density, n_0, has a value of ~ 10^{15} /m^3.

3.2.1.1. Equations

The equations that have to be solved to simulate the planar part of our problem are given by equations (3.2.1) – (3.2.3).

Poisson's Equation:

$$\frac{\partial^2 \Phi}{\partial x^2} = -\frac{en}{\varepsilon_0}. \qquad (3.2.1)$$

Continuity Equation:

$$\frac{\partial n}{\partial t} + \nabla(un) = 0. \qquad (3.2.2)$$

Momentum Balance Equation:

$$\frac{\partial u}{\partial t} + u\frac{\partial u}{\partial x} = \frac{e}{m_i}E. \qquad (3.2.3)$$

In equations (3.2.1) – (3.2.3), Φ is the potential, e is the electric charge of an ion, u is the ion velocity, n is the ion density, ε_0 is the electric permittivity of free space, m_i is the mass of an ion, and E is the electric field between the electrodes.

3.2.1.2. Boundary and Initial Conditions

The boundary conditions to be imposed are given by equations (3.2.4) – (3.2.7).

$$x = 0, \qquad \Phi(0,t) = 0 \ , \tag{3.2.4}$$

$$x = L, \qquad \Phi(L,t) = -\Phi_0 , \tag{3.2.5}$$

$$x = 0, \qquad u(0,t) = 0 \ , \tag{3.2.6}$$

$$x = 0, \qquad n(0,t) = n_0 . \tag{3.2.7}$$

The initial conditions to be imposed are given by equations (3.2.8) and (3.2.9).

$$t = 0, \qquad u(x,0) = 0 , \tag{3.2.8}$$

$$t = 0, \qquad n(x,0) = \frac{n_0}{\pi} \times \left\{ \arctan\left[50000 \times \left(x_j - 10^{-3} \right) \right] + \tfrac{\pi}{2} \right\}. \tag{3.2.9}$$

3.2.2. Numerical Procedure

Equations (3.2.1) – (3.2.3), which are subject to the boundary and initial conditions given by equations (3.2.4) – (3.2.9), have been solved numerically using a finite-differences technique. The computational domain is estimated to be between $x = 0$ and $x = L$, which is illustrated by figure 3.1.

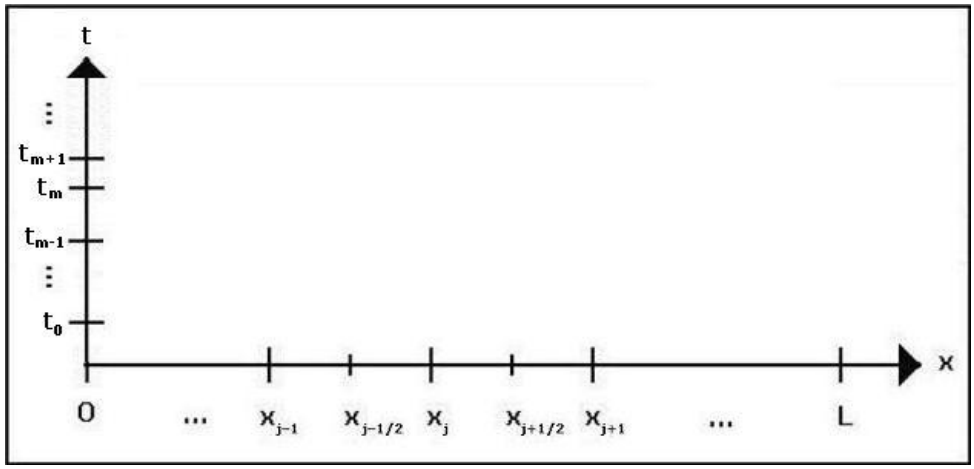

Figure 3.1: Computational domain

A uniform vertex-centered grid

$$x_j = j\Delta x, \quad \Delta x = L/N, \quad j = 0,1,..,N \tag{3.2.10}$$

is used where *j* is the spatial index.

The time level is given by

$$t_m = m\Delta t_m, \quad \Delta t_m > 0, \quad m = 0,1,.. \tag{3.2.11}$$

where subscript m denotes the time level t_m with a step size $\Delta t_m = t_m - t_{m-1}$.

Density n and electric potential Φ are evaluated at the nodes of the grids, while the ion velocity u and the electric field E are at the centers of the computational cells.

3.2.2.1. Poisson's Equation

To obtain a finite-differences approximation of Poisson's equation (3.2.1), which has the boundary conditions given by equations (3.2.4) and (3.2.5), a standard second order discrete scheme of the form given by equation (3.2.12) is used.

$$\frac{\partial^2 \Phi(x_j, t_m)}{\partial x^2} \approx \frac{\Phi^m_{j-1} - 2\Phi^m_j + \Phi^m_{j+1}}{(\Delta x)^2} + O\left((\Delta x)^2\right). \qquad (3.2.12)$$

As a result, Poisson's equation turns to the standard three-point problem given by equation (3.2.13).

$$-\Phi^m_{j-1} + 2\Phi^m_j - \Phi^m_{j+1} = \frac{en^{m-1}_j}{\varepsilon_0}(\Delta x)^2 \qquad (3.2.13)$$

Equation (3.2.13) is solved by the Thomas algorithm, using boundary conditions described in equations (3.2.4) and (3.2.5) in discrete form, which is given by equations (3.2.14) and (3.2.15).

$$\Phi^m_1 = 0 \qquad (3.2.14)$$

$$\Phi^m_N = -\Phi_0 \qquad (3.2.15)$$

3.2.2.2. Continuity Equation

To obtain a finite-differences representation of equation (3.2.2), it is first integrated over the cell volume $x_{j-1/2} \le x \le x_{j+1/2}$. As a result, we have

$$\frac{dn_j}{dt} = \frac{(un)_{j-1/2} - (un)_{j+1/2}}{\Delta x} \qquad (3.2.16)$$

where u is the ion velocity and n is ion density.

A choice of $n_{j\pm1/2}$ at the centers of the computational cells determines the concrete discretization method for the convective terms of equation (3.2.1). We used the third-order upwind-biased scheme [27], which has the form

$$(un)_{j+1/2} = \frac{1}{6}\left[u^{+}_{j+1/2}\left(-n_{j-1} + 5n_j + 2n_{j+1}\right) + u^{-}_{j+1/2}\left(2n_j + 5n_{j+1} - n_{j+2}\right)\right] \quad (3.2.17)$$

where

$$u^{+}_{j+1/2} = \max\left(0, u_{j+1/2}\right), \text{ and } u^{-}_{j+1/2} = \max\left(0, u_{j+1/2}\right). \quad (3.2.18)$$

For the numerical time integration, the extrapolated second order backward differentiation formula (BDF2) is used [28]:

$$\frac{3}{2}n^m - 2n^{m-1} + \frac{1}{2}n^{m-2} = \Delta t_m F(t_m, 2n^{m-1} - n^{m-2}),\ m \geq 2. \quad (3.2.19)$$

Here, F contains the discretized convective terms. Note, that spatial indices in equation (3.2.19) have been dropped.

Since two-step method needs n^0 and n^1 as starting values, the explicit Euler method given by equation (3.2.20) is used on the first step.

$$n^m = n^{m-1} + \Delta t_m F(t_m, n^{m-1}) \quad (3.2.20)$$

Because of the explicit time integration, we are restricted by the standard CFL condition for stability.

3.2.2.3. Momentum Balance Equation

Let us consider the momentum equation, which is given by equation (3.2.3). This equation can be rewritten in the form of

$$\frac{\partial u}{\partial t}+\frac{\partial}{\partial x}\left(\frac{u^2}{2}\right)=\frac{e}{m_i}E\,. \tag{3.2.21}$$

To have a conservative difference scheme for (3.2.3), it is constructed by the integro-interpolated method; integrating equation (3.2.3) over the computational cell $x_{j-1}\le x\le x_j$ equation (3.2.22) is obtained.

$$\int_{x_{j-1}}^{x_j}\left(u^m-u^{m-1}\right)dx+\frac{1}{2}\int_{t_{m-1}}^{t_m}\left(u_j^2-u_{j-1}^2\right)dt=\frac{e}{m_i}\int_{t_{m-1}}^{t_m}\int_{x_{j-1}}^{x_j}E dx dt \tag{3.2.22}$$

Different approximations of the integrals in equation (3.2.22) lead to different difference schemes. One of them is a scheme implicit in time and of the following form:

$$\frac{u_j^m-u_j^{m-1}}{\Delta t_m}+\frac{1}{2}\frac{\left(u_j^m\right)^2-\left(u_{j-1}^m\right)^2}{\Delta x}=f_j^m \tag{3.2.23}$$

with

$$f_j^m=\frac{e}{m_i}E(t_m,x_j)\,. \tag{3.2.24}$$

It is obvious that equation (3.2.23) represents a quadratic algebraic equation with respect to u_j^m. Using the ion velocity known from the previous time level u_j^{m-1}

($j = 1,2,...,N$), a numerical procedure can be organized by a successive calculation of u_j^m starting from the left boundary ($x = 0$)

$$u_1^m = 0 \tag{3.2.25}$$

to the right by the equation

$$u_j^m = -\frac{\Delta x}{\Delta t_{m-1}} + \sqrt{\frac{\Delta x^2}{\Delta t_{m-1}{}^2} + \frac{2\Delta x}{\Delta t_{m-1}} u_j^{m-1} + \left(u_{j-1}^m\right)^2 + 2\Delta x f_j^m} \tag{3.2.26}$$

where $j = 2,3,...,N$, $m = 1,2,3,...$

3.2.3. Numerical Results

Numerical procedure is organized as follows. On every new m^{th} time step, first, Poisson's equation is solved, using the known ion density n^{m-1} in its source term; hence, electric field in the new time step is determined. Then, the momentum balance equation is solved, using the known electric field, E^m, and the ion velocity in the new time step is determined. Finally, the continuity equation is solved, using the known ion velocity and therefore the ion density in the new time step, n^m, is determined.

The numerical convergence is checked by performing several calculations using refinement of the space grid and different time stepping parameters. The number of grid nodes used in the calculations was 200.

In the simulation, the ions are assumed to be titanium ions and the ion mass is taken to be $48.00 \times 1.67 \times 10^{-27}$ kg, the magnitude of the distance between the electrodes, L, is taken to be ~ 1.00×10^{-2} m, the negative potential applied to the cathode, Φ_0, is taken to be ~ 20.00 kV, potential applied to the anode is taken to

be 0.00 kV, the initial ion velocity is taken to be 0.00 m/s and the initial ion density, n_0, is taken to be ~ 1.00×10^{15} /m^3

The data obtained from the simulation is used to plot the ion density versus position graph and ion velocity versus position graph at a particular time. Figure 3.2 shows these graphs at the instants $t=\frac{t_{max}}{4}$, $t=\frac{t_{max}}{2}$, $t=\frac{3t_{max}}{4}$ and $t=t_{max}$.

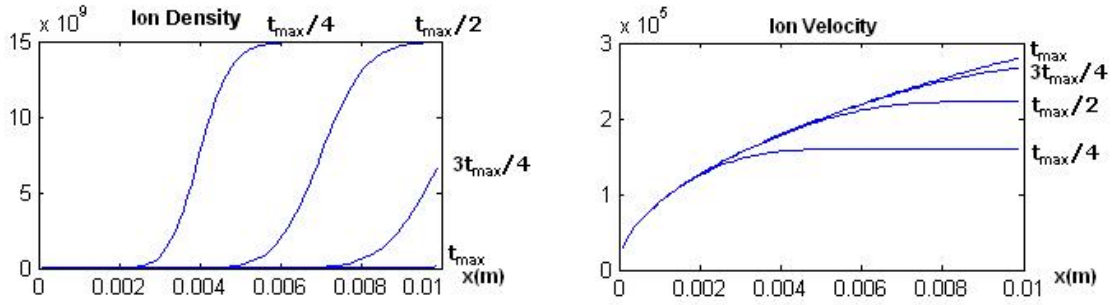

Figure 3.2: Ion density and ion velocity as a function of x at the instants $t=\frac{t_{max}}{4}$, $t=\frac{t_{max}}{2}$, $t=\frac{3t_{max}}{4}$ and $t=t_{max}$.

It can be easily seen from figure 3.2 that the ions at a particular position x move with almost the same velocity as they are accelerated towards the target. The motion of the matrix sheath and the position of the sheath edge can be seen from the density versus position graph in figure 3.2.

The implantation of ions ends, i.e. the ion matrix sheath disappears, at a time t_{max}, which is found as 7.08×10^{-8} s in the analytical calculations and 6.90×10^{-8} s in the simulation. The final ion velocity at $x=L$ and $t=t_{max}$ is obtained as 2.80×10^5 m/s from the simulation data. The analytically calculated final ion velocity, which

is 2.78×10^5 m/s, is approximately equal to the simulation result with an error of 0.71 %. It is also observed from figure 3.2 that the ion velocity inside the ion matrix at a particular instant is almost linear. However, the ion velocity versus position graphs plotted by using the analytical data, figure 3.3, and the numerical data, figure 3.2, indicate different relations between the ion velocity and position. The graphs of the analytical data indicate a linear relationship between ion velocity and position whereas the graphs of the numerical data indicate a curvilinear relationship between ion velocity and position. This linearization of analytically calculated ion velocity is due to the approximations made in the analytical calculations. This causes the analytically calculated ion velocity to increase more slowly than the simulated velocity in the time interval $0 < t < \frac{3t_{\max}}{4}$ and to catch the simulated values in the time interval $\frac{3t_{\max}}{4} < t < t_{\max}$.

The graph in figure 3.4 gives the analytically calculated ion velocity as a function of position and time.

Although the analytically calculated ion velocity is slightly different from the simulated ion velocity regarding the dependence on position, it can be concluded that there is a good agreement between the analytical and the numerical solutions.

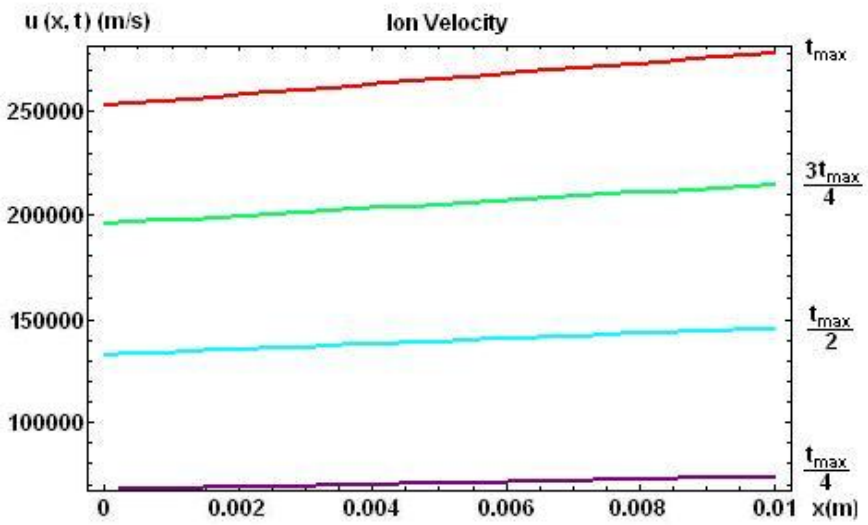

Figure 3.3: Ion velocity versus position graphs plotted using analytical results.

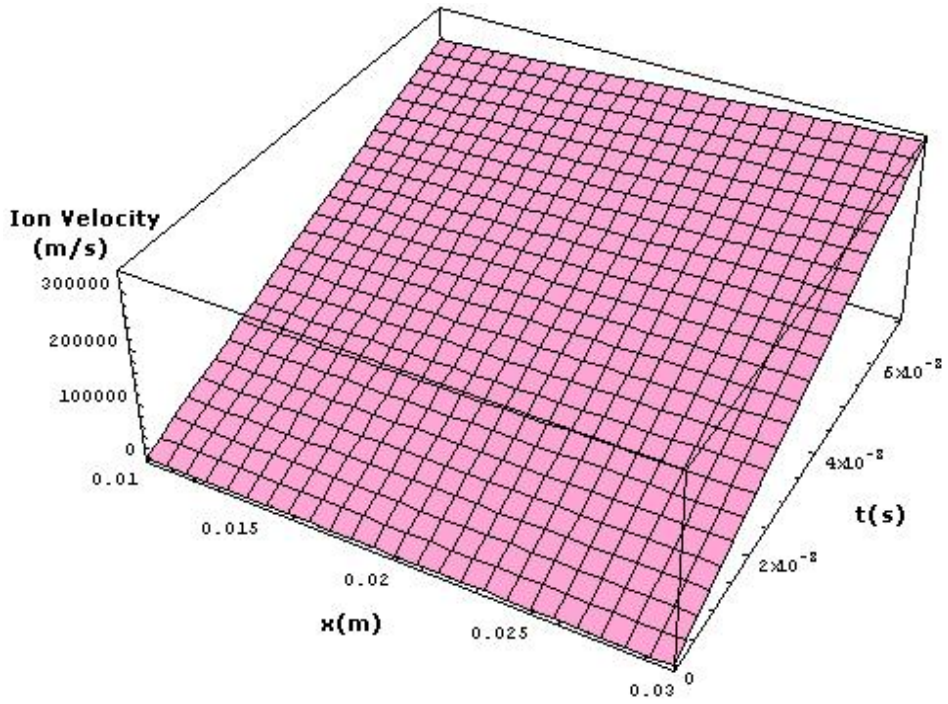

Figure 3.4: The analytically calculated ion velocity as a function of position and time.

3.3. CYLINDRICAL CONFIGURATION

3.3.1. The Model

The model presented here is a one-dimensional model, with a cylindrical anode of infinite length and radius r_1 and a cylindrical cathode where the target to be implanted is placed. The target considered is the internal surface of an infinitely long cylinder whose inner radius is r_2. The anode is axially placed inside the target. The magnitude of r_1 is ~10^{-2} m, r_2 is ~ 3×10^{-2} m, the negative potential applied to the cathode, Φ_0, is ~ 20 kV, whereas the anode is kept at zero potential. The ion velocity is initially zero and the initial ion density, n_0, has a value of ~10^{15}/m^3.

3.3.1.1. Equations

The equations that have to be solved to simulate the cylindrical part of our problem are given by equations (3.3.1) – (3.3.3).

Poisson's Equation:

$$\frac{1}{r}\frac{\partial}{\partial r}\left(r\frac{\partial \Phi}{\partial r}\right) = -\frac{en}{\varepsilon_0}. \qquad (3.3.1)$$

Continuity Equation:

$$\frac{\partial n}{\partial t} + \frac{1}{r}\frac{\partial}{\partial r}(run) = 0. \qquad (3.3.2)$$

Momentum Balance Equation:

$$\frac{\partial u}{\partial t} + u\frac{\partial u}{\partial r} = \frac{e}{m_i}E. \qquad (3.3.3)$$

In equations (3.3.1) – (3.3.3), Φ is the potential, e is the electric charge of an ion, u is the ion velocity, n is the ion density, ε_0 is the electric permittivity of free space, m_i is the mass of an ion, and E is the electric field between the electrodes.

3.3.1.2. Boundary and Initial Conditions

The boundary conditions to be imposed are given by equations (3.3.4) – (3.3.7).

$$r = r_1, \qquad \Phi(r_1, t) = 0, \tag{3.3.4}$$

$$r = r_2, \qquad \Phi(r_2, t) = -\Phi_0, \tag{3.3.5}$$

$$r = r_1, \qquad u(r_1, t) = 0, \tag{3.3.6}$$

$$r = r_1, \qquad n(r_1, t) = n_0. \tag{3.3.7}$$

The initial conditions to be imposed are given by equations (3.3.8) and (3.3.9).

$$t = 0, \qquad u(r, 0) = 0, \tag{3.3.8}$$

$$t = 0, \qquad n(r, 0) = \frac{n_0}{\pi} \times \left\{ \arctan\left[50000 \times \left(r_j - 10^{-3} \right) \right] + \tfrac{\pi}{2} \right\}. \tag{3.3.9}$$

3.3.2. Numerical Procedure

Equations (3.3.1) – (3.3.3), which are subject to the boundary and initial conditions given by equations (3.3.4) – (3.3.9), have been solved numerically using a finite-differences technique. The computational domain is estimated to be between the radius of anode, r_1, and the inner radius of cathode, r_2, where the distance between the electrodes is $r_2 - r_1 = L$. The computational domain is given by figure 3.5.

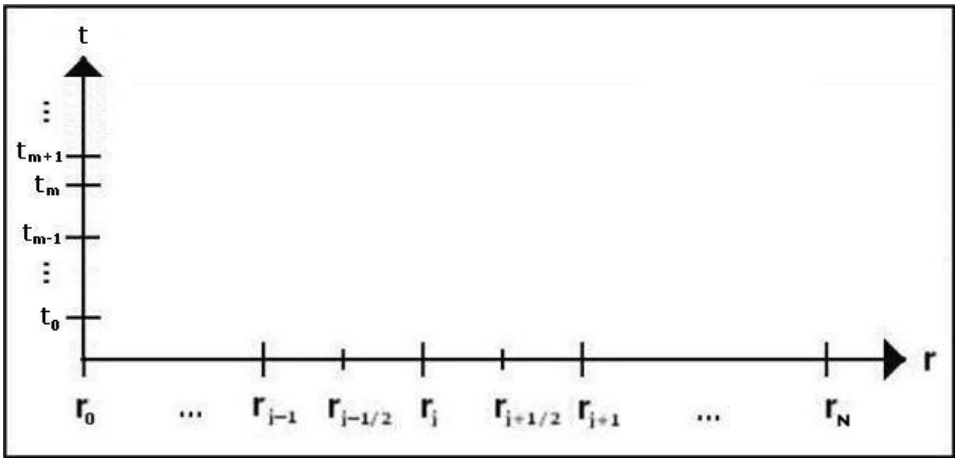

Figure 3.5: Computational domain

A uniform vertex-centered grid

$$r_j = j\Delta r, \quad \Delta r = L/N, \quad j = 0,1..,N \tag{3.3.10}$$

is used where *j* is the spatial index. The time level is given by equation (3.2.11).

Density n and electric potential Φ are evaluated at the nodes of the grids, while the ion velocity u and the electric field E are at the centers of the computational cells.

3.3.2.1. Poisson's Equation

To obtain a finite-differences approximation of Poisson's equation (3.3.1), which has the boundary conditions given by equations (3.3.4) and (3.3.5), the integro-interpolated method is used; integrating equation (3.3.1) over the computational cell $r_{j-1} \le r \le r_j$ equation (3.3.11) is obtained.

$$\frac{\partial^2 \Phi(r_j, t_m)}{\partial r^2} \approx \frac{r_{j-1/2}\Phi^m_{j-1} - 2r_j\Phi^m_j + r_{j+1/2}\Phi^m_{j+1}}{(\Delta r)^2} + O\left((\Delta r)^2\right) \qquad (3.3.11)$$

As a result, this problem turns to the standard three-point problem of the form (3.1.2) which is again solved by the Thomas algorithm using the formulation given by equations (3.2.13) – (3.2.15).

3.3.2.2. Continuity Equation

To obtain a finite-differences representation of equation (3.3.2), it is integrated it over the cell volume $r_{j-1/2} \le r \le r_{j+1/2}$ and equation (3.3.12) is obtained.

$$\frac{dn_j}{dt} = \frac{\frac{r_{j-1/2}}{r_j}(un)_{j-1/2} - \frac{r_{j+1/2}}{r_j}(un)_{j+1/2}}{\Delta r} \qquad (3.3.12)$$

The third-order upwind-biased scheme [27], which has a form given by equations (3.2.17) and (3.2.18), and the extrapolated second order BDF2 [28] given by equation (3.3.13) are used.

$$\frac{3}{2}n^m - 2n^{m-1} + \frac{1}{2}n^{m-2} = \Delta t_m F(t_m, 2n^{m-1} - n^{m-2}),\ m \ge 2, \qquad (3.3.13)$$

Since the two-step method requires n^0 and n^1 as starting values, the explicit Euler method, given by equation (3.2.20), is used again on the first step with the standard CFL condition for stability.

3.3.2.3. Momentum Balance Equation

Equation (3.3.3) can be rewritten in the form given by equation (3.2.21). The integro-interpolated method over the computational cell $r_{j-1} \le r \le r_j$ and the

scheme implicit in time given by equations (3.2.23) and (3.2.24) are again used in the numerical computation of momentum balance equation by a successive calculation of u_j^m starting from the left boundary ($r = r_1$) to the right by the equation (3.2.26).

3.3.3. Numerical Results

The numerical procedure is organized in the same form as the numerical procedure given in section 3.2.3.

In the simulation, the ions are assumed to be titanium ions and the ion mass is taken to be $48.00 \times 1.67 \times 10^{-27}$ kg, the radius of the anode, r_1, is taken to be ~ 1.00×10^{-2} m, the inner radius of the cathode, r_2, is taken to be ~3.00×10^{-2} m, the magnitude of the distance between the electrodes, L, is taken to be ~2.00×10^{-2} m, the negative potential applied to the cathode, Φ_0, is taken to be ~ 20.00 kV, potential applied to the anode is taken to be 0.00 kV, the initial ion velocity is taken to be 0.00 m/s and the initial ion density, n_0, is taken to be ~ 1.00×10^{15} /m^3.

The data obtained from the simulation is used to plot the ion density versus position graph and ion velocity versus position graph at a particular time. Figure 3.6 shows these graphs at the instants $t = \frac{t_{\max}}{4}$, $t = \frac{t_{\max}}{2}$, $t = \frac{3t_{\max}}{4}$ and $t = t_{\max}$.

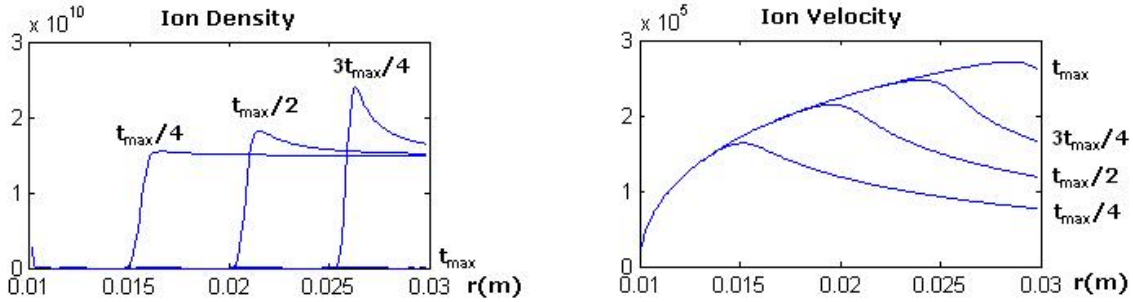

Figure 3.6: Ion density and ion velocity as a function of r at the instants $t = \frac{t_{\max}}{4}$, $t = \frac{t_{\max}}{2}$, $t = \frac{3t_{\max}}{4}$ and $t = t_{\max}$.

It can easily be seen from figure 3.6 that the ions at a particular r move with almost the same velocity as they are accelerated towards the target. The motion of the matrix sheath and the position of the sheath edge can be seen from the density versus position graph in figure 3.6.

The implantation of ions ends, i.e. the ion matrix sheath disappears, at a time $t_{\max}$, which is found as 1.05×10^{-7} s in the analytical calculations and 1.25×10^{-7} s in the simulation. This difference is caused because the first order sheath edge, $s^{(1)}(t)$, has been ignored since its contribution to the ion velocity is second order. The final ion velocity is obtained as 2.71×10^{5} m/s from the simulation data. The analytically-calculated final ion velocity, which is 2.75×10^{5} m/s, is approximately equal to the simulation result with an error of 1.47 %. In addition to this, the ion velocity versus position graph plotted by using the analytical data, which is shown in figure 3.7, and the numerical data indicate similar relationships between ion velocity and position.

It can be concluded that there is a good agreement between analytical and numerical solutions.

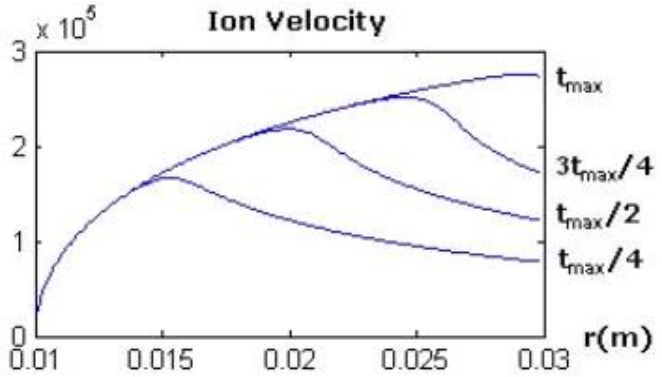

Figure 3.7: Ion velocity as a function of r at four particular instants $t = \frac{t_{\max}}{4}$, $t = \frac{t_{\max}}{2}$, $t = \frac{3t_{\max}}{4}$ and $t = t_{\max}$.

CHAPTER 4

CONCLUSION

Plasma source ion implantation (PSII), which was invented by Conrad in 1987 [13], is a well-established plasma-based manufacturing technique, which is frequently used in the surface modification of materials for industrial applications [1, 3, 4].

PSII is a room temperature surface enhancement technique that uses a plasma medium surrounding a target and high-negative-voltage, high-current pulses to accelerate ions into a target surface from all directions. PSII modifies the target surface in beneficial ways, making it harder, improving wear properties, reducing the coefficient of friction, enhancing its resistance to corrosion and dramatically improving the wear-life of manufacturing tools in actual industrial applications [9, 14].

In this work, the dynamic ion behavior during the evolution of the ion matrix sheath, considering the industrial application plasma source ion implantation for both planar and cylindrical targets, is treated analytically and a code that simulates this dynamic ion behavior numerically is developed.

It is known that if the separation between the electrodes in a discharge tube is small, upon the application of a large potential between the electrodes, an ion matrix sheath is formed, which fills the whole inter-electrode space. After a short time, the ion matrix sheath starts moving towards the cathode and disappears there. Two regions are formed as the matrix sheath evolves. We have derived the potential profiles of these two regions and estimated the ion flux on the cathode for the planar case. Then, by using the finite-differences method, the problem is simulated numerically.

For the planar case, the potential profile between the electrodes is calculated analytically and the results are given by equations (2.1.31) and (2.1.32) in the theory and calculations chapter. Then, using these potentials and the equation of motion of ions, the ion velocity is calculated analytically, equation (2.1.40), and the ion flux is estimated, given in equation (2.1.41). Using the analytical data, the ion velocity as a function of x at the instants $t = \frac{t_{max}}{4}$, $t = \frac{t_{max}}{2}$, $t = \frac{3t_{max}}{4}$, $t = t_{max}$ and the ion flux as a function of time at the cathode are plotted (figures 2.4, 2.5, 2.6, 2.7 and 2.8). It is observed both from the analytical results and their graphs that the ion velocity increases linearly with distance and the ion flux increases almost linearly with time.

Then, a code that simulates the ion behavior for the planar configuration as the ion matrix evolves is developed. The data obtained from the simulation is used to plot the ion density versus position graph and ion velocity versus position graph at four particular times, which is shown in figure 3.2 in the simulation chapter. It is observed from these graphs that the ions at a particular position move with almost the same velocity when they are accelerated towards the target. The motion of the matrix sheath and the position of the sheath edge can be seen from the density versus position graph.

The ion matrix sheath disappears, at a time t_{max}, which is found as 7.08×10^{-8} s in the analytical calculations and 6.90×10^{-8} s in the simulation. The final ion velocity at $x = L$ and $t = t_{max}$ is obtained as 2.80×10^{5} m/s from the simulation data. The analytically-calculated final ion velocity, which is 2.78×10^{5} m/s, is approximately equal to the simulation result with an error of 0.71 %. It is also observed from figure 3.2 that the ion velocity inside the ion matrix at a particular instant is almost linear. However, the ion velocity versus position graphs plotted by using the analytical data and the numerical data indicate a small difference in the relationships between ion velocity and position. The graphs of the analytical data indicate a linear relationship between ion velocity and position whereas the graphs of the

numerical data indicate a curvilinear relationship between ion velocity and position. This linearization of analytically-calculated ion velocity is due to the approximations made in the analytical calculations. This causes the analytically-calculated ion velocity to increase more slowly than the simulated velocity in the time interval $0 < t < \frac{3t_{\max}}{4}$ and to catch the simulated values in the time interval $\frac{3t_{\max}}{4} < t < t_{\max}$. Although the analytically-calculated ion velocity is slightly different from the simulated ion velocity regarding the dependence on position, it can be concluded that there is a good agreement between analytical and numerical solutions.

For the cylindrical case, the potential profile between the electrodes is calculated analytically and the results are given by equations (2.2.52) and (2.2.53) in the theory and calculations chapter. Then, using these potentials and the equation of motion of ions, the differential equations for the zeroth and first order ion velocities are derived. The zeroth order ion velocity is calculated analytically, which is given by equation (2.2.74) in the theory and calculations chapter. However, it is observed that equation (2.2.74), which is obtained analytically under the approximation (2.2.36), needs to be studied further because it does not fully satisfy equation (2.2.56). Therefore, the differential equations for the first order ion velocity and for the zeroth order ion velocity, equations (2.2.56) and (2.2.57), are solved numerically. The relationships between the ion velocity and position, and the ion flux and time are shown in the figures 2.17 and 2.18. It is observed both from the analytical results and their graphs that the ion velocity increases in a curvilinear manner with distance and the ion flux increases in a curvilinear manner with time.

Then, a code that simulates the ion behavior for the cylindrical configuration as the ion matrix evolves is developed. From the simulation data, it is observed that the ions at a particular r move with almost the same velocity when they are accelerated towards the target. The motion of the matrix sheath and the position of the sheath edge can be seen from the density versus position graph in figure 3.6

in the simulation chapter. The implantation of ions ends, i.e. the ion matrix sheath disappears, at a time t_{max}, which is found as 1.05×10^{-7} s in the analytical calculations and 1.25×10^{-7} s in the simulation. This difference is caused because the first order sheath edge, $s^{(1)}(t)$, has been ignored since its contribution to the ion velocity is second order. The final ion velocity is obtained as 2.71×10^{5} m/s from the simulation data. The analytically-calculated final ion velocity, which is 2.75×10^{5} m/s, is approximately equal to the simulation result with an error of 1.47 %. In addition to this, the ion velocity versus position graph plotted by using the analytical data and the numerical data indicate similar relationships between ion velocity and position. Therefore, it can be concluded that there is a good agreement between analytical and numerical solutions.

In this work, the constants, such as the inter-electrode separation, used in the calculations are chosen to be well-adjusted to the experimental values so that these calculations can be used in the experiments as a reference. In the calculations, the ions are assumed to be titanium ions.

To conclude, the dynamic ion behavior during the evolution of the ion matrix sheath has been analytically treated, considering the industrial application plasma source ion implantation for both planar and cylindrical targets, and then a code that simulates this dynamic ion behavior numerically is developed. It has been observed that the results of both the analytical calculations and the numerical simulations are in a good agreement.

REFERENCES

[1] Demokan, O., Critical Analysis of Matching Schemes in Capacitively Coupled Discharges, IEEE Transactions on Plasma Science, **31**, 1100 (2003).

[2] Lawrence Livermore National Laboratory (LLNL), (1999), Plasma Dictionary, Retrieved January, 2006, from: http://plasmadictionary.llnl.gov/terms.lasso?-MaxRecords=1&-SkipRecords=16&-SortField=Term&-SortOrder=ascending&-Op=bw&ABC=P&page=detail.

[3] Conrad, J. R., Radke, J. L., Dodd, R. A., and Worzala, F. J., Plasma Source Ion Implantation Technique For Surface Modification Of Materials, J. Appl. Phys., **62**, 4951 (1987).

[4] Filiz, Y., Ion Implantation in Planar Targets with Semi-Cylindrical Grooves, M.S. Thesis, Middle East Technical University (2002).

[5] Demokan, O., Ion-Matrix Sheaths Inside Cylindrical Bores with Small Radii and Longitudinal Grooves, IEEE Transactions on Plasma Science, **32**, 316 (2004).

[6] Demokan, O., Ion-Matrix Sheaths Related To Planar Targets with Semicylindrical Grooves, J. Appl. Phys., **93**, 83 (2003).

[7] Demokan, O., Ion-Matrix Sheaths Related To Targets with Grooves, J. Appl. Phys., **91**, 5587 (2002).

[8] Demokan, O., Ion Implantation and Deposition on the Inner Surfaces of Cylinders by Exploding Metallic Foils, IEEE Transactions on Plasma Science, **28**, 1720 (2000).

[9] Roth, J.R., Industrial Plasma Engineering: Volume II, Bristol and Philadelphia: Institute of Physics Publishing (2001).

[10] Los Alamos National Laboratory (LANL), (1998), Plasma Source Ion Implantation Research, Development, and Applications, Retrieved January, 2006, from: http://www.lanl.gov/p/pdfs/pr/pr_97_98/psii.pdf.

[11] Conrad, J. R., Sheath Thickness and Potential Profiles of Ion- Matrix Sheaths for Cylindrical and Spherical Electrodes, J. Appl. Phys., **62**, 777 (1987).

[12] Conrad, J. R., Castagna, T., Plasma Source Ion Implantation for Surface Modification, Bull. Amer. Phys. Soc., **31**, 1479 (1986).

[13] Widner, M. A., Alexeff, I., Jones, W. D., Langmuir Sheath Thickness as Observed by Ion-Acoustic Waves and a Hot Probe, J. Appl. Phys., **43**, 1532 (1972).

[14] Widner, M. A., Alexeff, I., Jones, W. D., Lonngren, K. E., Ion Acoustic Wave Excitation and Ion Sheath Evolution, Phys. Fluids, **13**, 2532 (1970).

[15] Alexeff, I., Jones, W. D., Transient Plasma Sheath Discovered By Ion Acoustic Waves, Phys. Fluids, **12**, 345 (1969).

[16] Lieberman, M. A., Lichtenberg, A. J., Principles of Plasma Discharges and Materials Processing, John Wiley & Sons (1994).

[17] Sheridan, T. E., Ion-matrix sheath in a cylindrical bore, J. Appl. Phys., **74**, 4903 (1993).

[18] Zeng, X., Tang, B., Chu, P. K., Improving the plasma immersion ion implantation impact energy inside a cylindrical bore by using an auxiliary electrode, Appl. Phys. Lett., **69**, 3815 (1996).

[19] Wikimedia Foundation, Inc., (2005), Numerical Analysis, Retrieved January, 2006, from: http://en.wikipedia.org/wiki/Numerical_analysis.

[20] Leonardo Volpi, (2006), Spreadsheet Finite Differences Method, Retrieved January, 2006, from: http://digilander.libero.it/foxes/diffequ/iterative_method.htm.

[21] SILUX LTD., (2006), Frequently Asked Questions, Retrieved January, 2006, from: http://www.silux.com/faq2.cfm.

[22] Assoc. Prof. Richard Fitzpatrick from University of Texas, (2003), The Lax Scheme, Retrieved January, 2006, from: http://farside.ph.utexas.edu/teaching/329/lectures/node105.html.

[23] Computer Simulation of Quantum Mechanics - Porthouse, (2005), The Courant-Friedrichs-Levy Condition, Retrieved January, 2006, from: http://ourworld.compuserve.com/homepages/anima/cfl.htm.

[24] Network on the Integrity Assessment of Large Concrete Dams Project Group, (2004), Boundary Value Problems Analysis Techniques: Finite Differences Method, Retrieved January, 2006, from: http://nw-ialad.uibk.ac.at/Wp2/Tg3/Se4/Ss7.

[25] Online Center for Computational Fluid Dynamics, (2005), Tridiagonal Matrix Algorithm – TDMA (Thomas Algorithm), Retrieved January, 2006, from: http://www.cfd-online.com/Wiki/Thomas_algorithm.

[26] Morton, K. W., Mayers, D. F., Numerical Solution of Partial Differential Equations, Cambridge University Press, (1994).

[27] Hundsdorfer, W., Verwer, J. G., Numerical Solution of Time-Dependent Advection-Diffusion-Reaction Equations: Springer Series in Computational Mathematics 33, Springer (2003).

[28] Wesseling, P., Principles of Computational Fluid Dynamics: Springer Series in Computational Mathematics 29, Springer (2001).